Environmental Influences on the Strength of Tropical Storm Debby (2006)

JASON A. SIPPEL,* SCOTT A. BRAUN, AND CHUNG-LIN SHIE*

Laboratory for Atmospheres, NASA Goddard Space Flight Center, Greenbelt, Maryland

(Manuscript received 16 August 2010, in final form 30 June 2011)

ABSTRACT

This study uses mesoscale ensemble forecasts to compare the magnitude of nonaerosol effects of the Saharan air layer (SAL) with other environmental influences on the intensity of Tropical Storm Debby. Debby was a weak Cape Verde storm that dissipated over the tropical North Atlantic a few days after forming in August 2006. The system has received considerable attention because of its vicinity to the SAL as it struggled to intensify, which has led to speculation that the SAL helped lead to the storm's demise. Statistical correlation is used to better understand why some ensemble members strengthen the pre-Debby wave into a hurricane and others develop only a weak vortex.

Although the results here suggest that the SAL slowed intensification during the predepression to depression stages, it was not likely responsible for Debby's dissipation. The most obvious SAL-related factor to affect long-term intensity in the ensembles is dry air above 2 km, which delays organization of the low-level vortex. Warm temperatures within the SAL and shear associated with the African easterly jet (AEJ) exhibit a weak, secondary relationship with forecast intensity variability. An important result here is that sensitivity to the dry environmental air depends considerably on cyclone strength, and it becomes insignificant once a tropical storm forms. Furthermore, Debby's most rapid period of intensification coincided with its track over somewhat higher sea surface temperatures, and intensification ended when the storm moved over cooler waters. The results herein suggest that this factor might have affected the storm's intensity more strongly than did any effect of the SAL. Even later, subsequent to the period examined by these ensembles, Debby dissipated under the influence of stronger vertical wind shear from an upper-level trough.

These results show that the relationship among the SAL, AEJ, and developing tropical cyclones is not as straightforward as has been hypothesized by some recent studies. Ultimately, the nuanced relationship between storm intensity and the SAL shows that much care needs to be taken before drawing conclusions about the effect of the SAL on any particular cyclone. The authors therefore advocate more rigorous future analysis through both idealized and ensemble studies to more fully quantify the effect of the SAL on tropical cyclones in general.

1. Introduction

Considerable debate has recently evolved regarding the potential impacts of the Saharan air layer (SAL) on tropical cyclone genesis and intensification. The SAL, which is an elevated mixed layer with warm temperatures and low relative humidity, forms when westward-moving air crosses the Saharan desert and overrides cooler marine air over the Atlantic Ocean (Carlson and Prospero 1972; Prospero and Carlson 1981; Karyampudi and Carlson 1988). Early studies (e.g., Karyampudi and Carlson 1988; Karyampudi and Pierce 2002) suggested that the SAL positively influences the growth of African easterly waves (AEWs) and tropical cyclones in the Atlantic. However, a more recent study by Dunion and Velden (2004, hereafter DV04) suggested that increased vertical wind shear, dry low–midlevel air, and a strong low-level inversion associated with the SAL inhibit tropical cyclone formation and intensification. Although a number of recent studies have concurred with these findings for both individual systems (Wu et al. 2006; Jones et al. 2007; Shu and Wu 2009; Vizy and Cook 2009; Reale et al. 2009) and whole seasons (Lau and Kim 2007a,b; Sun et al. 2008), the results of Braun (2010a,b) and Braun et al.

* Additional affiliation: Goddard Earth Sciences and Technology Center, University of Maryland, Baltimore County, Baltimore, Maryland.

Corresponding author address: Dr. Jason A. Sippel, NASA GSFC, Code 613.1, Greenbelt, MD 20771.
E-mail: jason.sippel@nasa.gov

DOI: 10.1175/2011JAS3648.1

© 2011 American Meteorological Society

(2011, hereafter BSN11) call into question the hypothesized negative impacts on tropical cyclones. In particular, Braun (2010a) suggested that a large fraction of the dry air over the central and eastern Atlantic Ocean is not of Saharan origin but is instead caused by large-scale subsidence. Braun (2010a,b) also showed that dry air near several individual systems was unrelated to the SAL, while BSN11 demonstrated that dry air of any origin above the boundary layer does not readily entrain into the tropical cyclone inner core in the absence of storm-relative flow or cyclone asymmetries.

Tropical Storm Debby, which developed off the coast of Africa in August 2006, has received considerable attention because of its development during the National Aeronautics and Space Administration's (NASA) African Monsoon Multidisciplinary Analysis (NAMMA) field campaign and because of its vicinity to possible SAL air as it struggled to intensify. Jenkins and Pratt (2008) and Jenkins et al. (2008) suggested that Saharan dust associated with SAL outbreaks invigorated convection in outer rainbands as Debby developed, though the effect on cyclone strength due to this factor is unclear. Zipser et al. (2009) described observations of Debby in some detail, noting a strongly titled vortex several days after genesis, which is consistent with a sheared environment. They also speculated that the dry air surrounding Debby had SAL origins, although they made no statements regarding the effects of this air on Debby's strength. Meanwhile, the postanalysis tropical cyclone report issued by the National Hurricane Center (NHC) mentioned the dry, stable air mass surrounding Debby as a leading factor in its failure to intensify beyond a moderate tropical storm. Shu and Wu (2009) went a step further and speculated that dry SAL air was directly related to Debby's weakening. However, Debby was one of several storms investigated by Braun (2010a), who found that much of the driest air surrounding the system was of non-Saharan origin. Thus, there are conflicting ideas regarding the role of the SAL in Debby's evolution.

The intent of this paper is to use ensemble simulations in a manner similar to Sippel and Zhang (2008, 2010, hereafter SZ08 and SZ10) to compare the potential effects of the thermodynamic and kinematic characteristics of the SAL with other environmental influences on Debby's intensification. Those studies respectively examined ensemble sensitivity in a nondeveloping null case and a disturbance that rapidly intensified to a hurricane, both of which occurred in the Gulf of Mexico. Both studies found that variability in moisture and atmospheric stability were leading causes of cyclone intensity spread and that moisture availability was more important to genesis than instability. Thus, by similarly investigating the sources of intensity spread in an ensemble forecast of Debby, one can gain insight into some of the factors that affected Debby's genesis and intensification.

The remainder of this study proceeds as follows. Section 2 examines Debby's synoptic background and evolution, and section 3 describes our methods. Sections 4 and 5 respectively present results from a control ensemble (CTRL) and sensitivity tests from an ensemble with weaker storms (WEAK). To better understand the extent to which Debby was surrounded by SAL air, section 6 examines trajectories from several ensemble members of CTRL. Finally, a summary and conclusions are found in section 7.

2. Background

Tropical Storm Debby formed from a tropical wave just off the coast of Africa in August 2006. The National Centers for Environmental Prediction (NCEP) final analysis (FNL) in Fig. 1 indicates that the axis of the wave at 3 km was several hundred kilometers east of the African coast at 0000 UTC 20 August. Nearer the surface, the increase in 2-km potential vorticity (PV) and development of a weak circulation by 20 August (Figs. 2a,b) suggests the possible influence of convection in building a low-level vortex (e.g., Haynes and McIntyre 1987; Raymond and Jiang 1990). Indeed, the Tropical Rainfall Measuring Mission (TRMM) multisatellite precipitation analysis (Huffman et al. 2007) in Fig. 3a shows widespread precipitation associated with this system before it emerged over the Atlantic. Convection continued over the next several days (Figs. 3b,c), and Figs. 1c and 2c,d indicate that the low-level vortex amplified considerably. As noted by Vizy and Cook (2009), the disturbance developed in a region of high relative humidity (Figs. 1a,c), which also favored surface vortex development. The NHC tropical cyclone report (TCR) estimates that a tropical depression formed at 1800 UTC 21 August south-southeast of the Cape Verde Islands (Figs. 4 and 5) and that Tropical Storm Debby formed by 0000 UTC 23 August.

The 24-h period beginning 1200 UTC 22 August, which approximately corresponds to when the storm encountered slightly warmer sea surface temperatures (SSTs), encompassed the most rapid intensification of this system (see the thick section of Debby's observed track in Fig. 4). According to the NHC TCR the minimum sea level pressure (SLP) during this period dropped by 6 hPa (Fig. 5), and the maximum winds increased by about 7.5 m s^{-1} (not shown). Meanwhile, the NASA DC8 aircraft investigating the storm on 23 August as part of the NAMMA campaign found that the storm had organized quite quickly. In particular, they found a well-defined low–midlevel eye in radar reflectivity around 1700 UTC 23 August and 30 m s^{-1} winds at 700 hPa (Zipser et al. 2009).

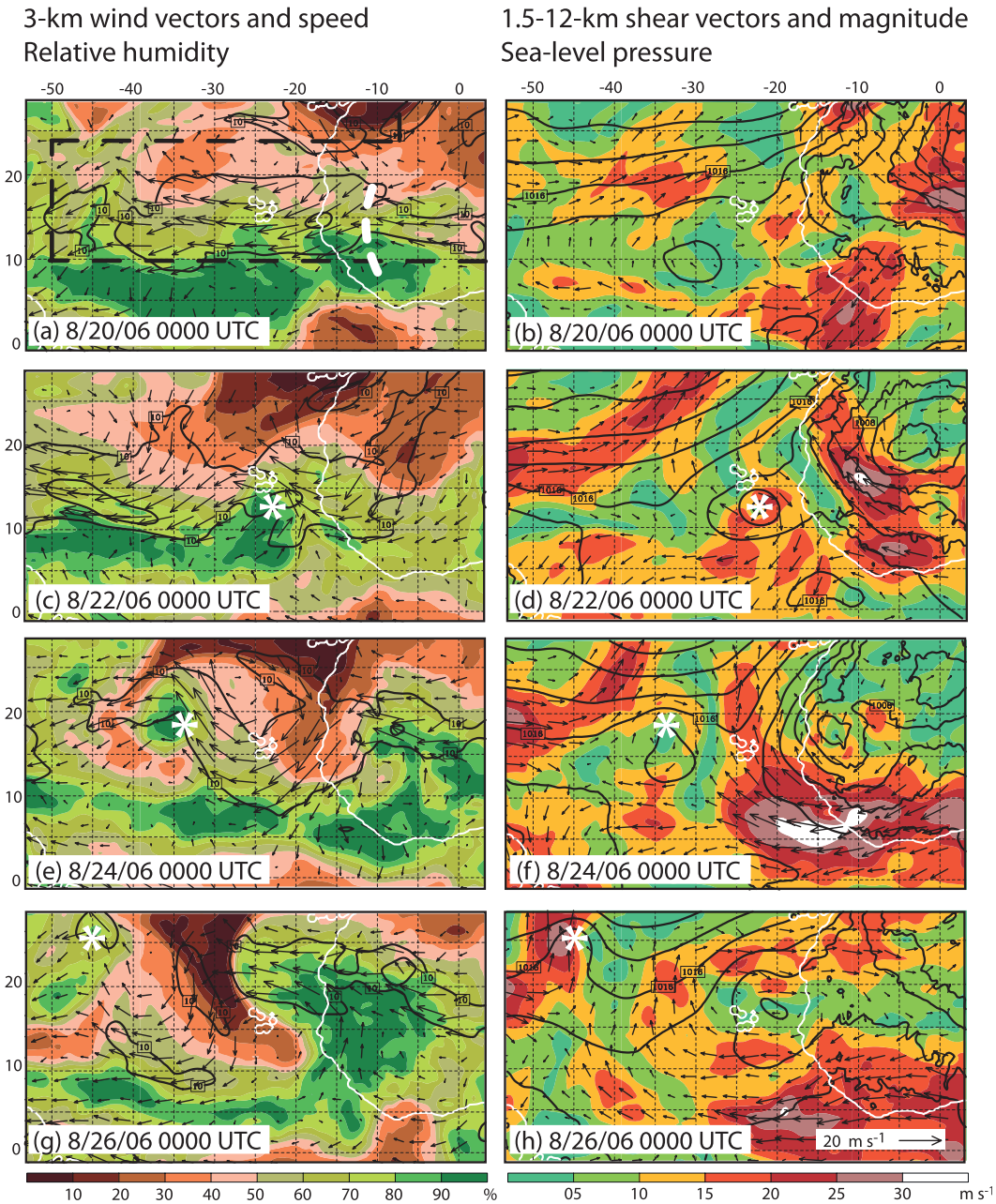

FIG. 1. FNL analyses of winds, relative humidity, sea level pressure, and wind shear during the pre-Debby disturbance and Debby: (left) 3-km wind vectors, wind speed (contoured every 10 m s^{-1}), and relative humidity (color filled every 10%) at 0000 UTC on (a) 20, (c) 22, (e) 24, and (f) 26 August and (right) sea level pressure (contoured every 4 hPa), 1.5–12-km (~200–850-hPa) wind shear magnitude (color filled every 5 m s^{-1}), and shear vectors at the same times as in the left column. The dashed black line in (a) outlines the spatial region of potential SAL air for the trajectory analysis, and the dashed white line shows the axis of the pre-Debby wave. In (c)–(h) the analysis 1-km PV maximum is indicated with a white asterisk.

Despite Debby's rapid organization during 22–23 August, the system never strengthened beyond a moderate tropical storm. Figure 5 shows that the rate of intensification slowed considerably later on 23 August, at which time Fig. 4 shows the storm to have moved over somewhat cooler SSTs. The system is estimated to have reached peak intensity at 0600 UTC 24 August with maximum winds of 22.5 m s^{-1} and a minimum surface pressure of 999 hPa (Fig. 5). Thereafter, Debby slowly weakened and finally dissipated early on 28 August.

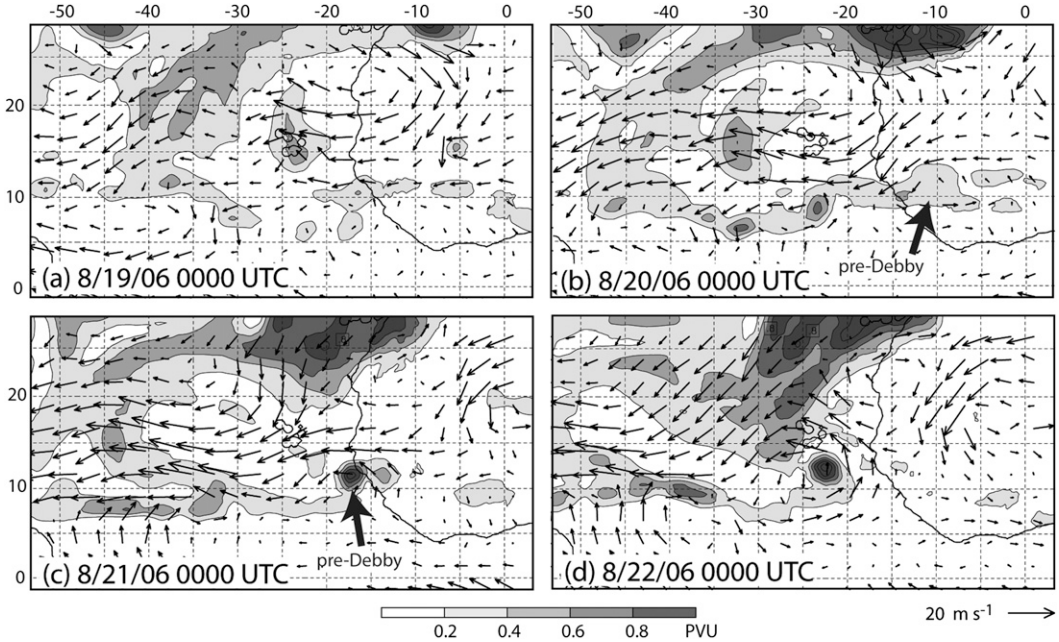

FIG. 2. FNL analyses of 2-km winds and PV at 0000 UTC on (a) 19, (b) 20, (c) 21, and (d) 22 August. The location of the pre-Debby disturbance is indicated with an arrow in (b) and (c).

The precise reason for Debby's failure to intensify is a matter of some debate. Without a doubt, Debby became increasingly surrounded by dry midlevel air (Fig. 1e), which has led some to believe that dry SAL air was responsible for the storm's demise (e.g., Shu and Wu 2009). However, as previously mentioned, the results of Braun (2010a) suggest that the dry air that increasingly wrapped around Debby's western and southern sides was not associated with the SAL. This conclusion was partly based on the Moderate Resolution Imaging Spectroradiometer (MODIS) dust product (Fig. 3), which shows that the very dry air south and west of the weakening Debby on 24–26 August had generally low aerosol optical depth (AOD) values (i.e., less than 0.2; Figs. 3f–h). Interestingly, Debby intensified most quickly while adjacent to very dusty SAL air on 22–23 August. Thus, it is not obvious that the SAL impacted Debby's intensity. Regardless of the SAL, whether or not the encircling dry air affected the storm's intensity has not been definitively shown in peer-reviewed literature.

There are several other potential explanations for Debby's lack of intensification and eventual dissipation. As was previously mentioned, the storm moved over increasingly cooler SSTs at roughly the same time that intensification slowed on 23 August. The system only marginally intensified thereafter as it approached the 26°C isotherm, which is thought to be near the lower limit favorable for tropical cyclone intensification (Gray 1968). Although Debby eventually did encounter warmer SSTs, the storm did not do so before encountering an increasingly hostile shear environment (Fig. 1). With the approach of an upper-level trough, the magnitude of 1.5–12-km (~850–200 hPa) vertical wind shear surrounding the center by 26 August was considerably larger than 12.5 m s^{-1}, which DeMaria et al. (2001) found to be the upper limit for a favorable intensification environment. Thus, it is likely that low SSTs helped cause Debby to stop intensifying and that excessive wind shear unrelated to the African easterly jet (AEJ) was a primary contributor to Debby's demise.

3. Methods

This study uses ensemble correlation to understand the storm dynamics, an idea that first appeared in peer-reviewed literature with Zhang (2005). Hawblitzel et al. (2007) refined this methodology to study a midlatitude mesoscale convective system, and SZ08 and SZ10 made further improvements in their studies of Gulf of Mexico tropical cyclones. Hakim and Torn (2008) used a similar method to study the dynamics of midlatitude cyclones, and Torn (2010) followed with a study of an AEW.

a. Forecast model and ensemble initialization

The Advanced Research version of the Weather Research and Forecasting model version 2.2 (WRF; Skamarock et al. 2005), is used to capture the evolution of the system, from the pre-Debby wave over Africa

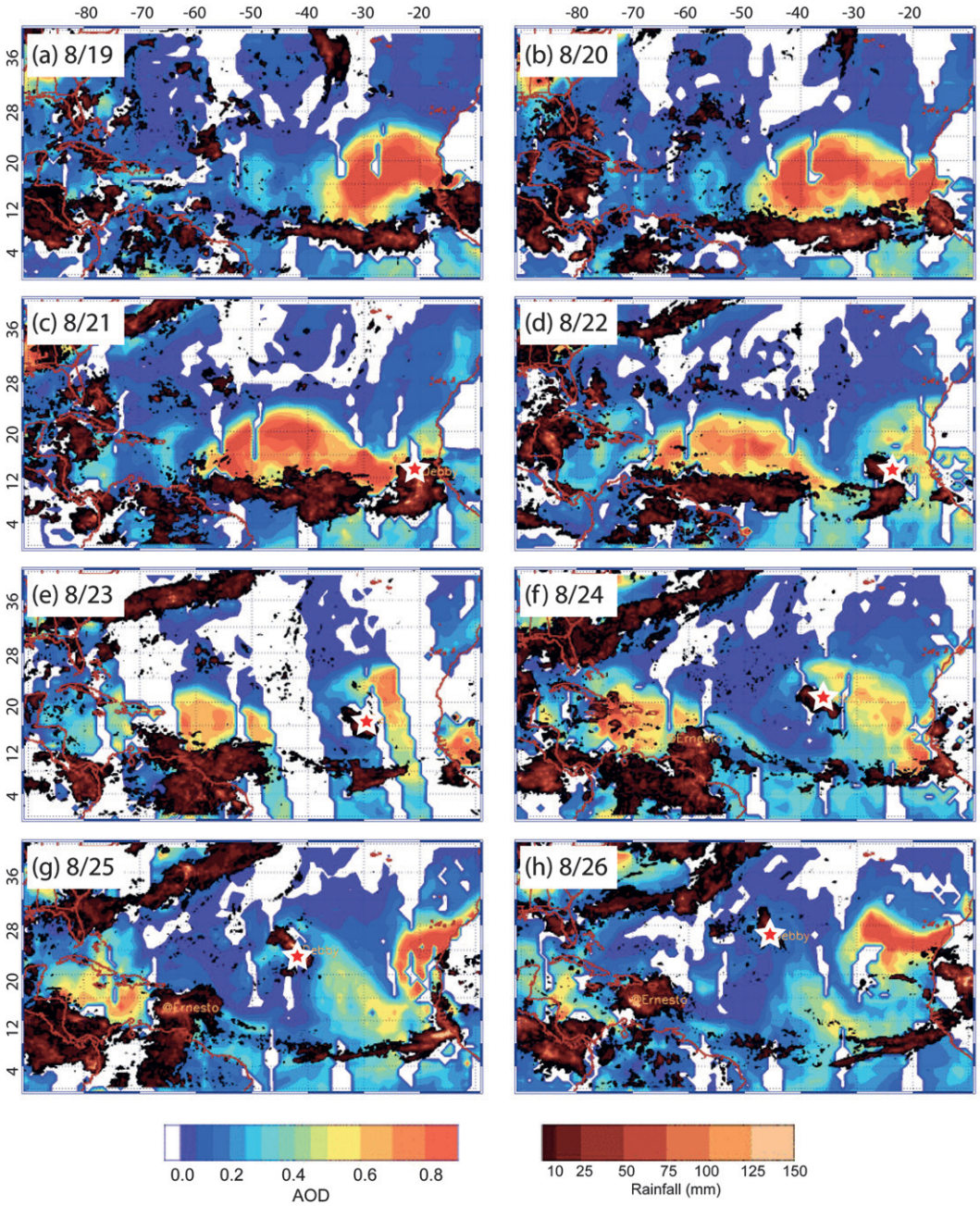

FIG. 3. MODIS AOD and TRMM 24-h accumulated rainfall for 19–26 August. The position of Debby is indicated by the red star. White areas indicate no AOD data.

through Debby's intensification over the eastern Atlantic (Figs. 4 and 5). The outer, 27-km WRF domain covers much of the tropical eastern Atlantic and interior Africa (Fig. 4) with 220 × 120 grid points, while the nested 9 km (3 km) domain concentrates more closely on the track of the wave and cyclone with 400 × 250 (991 × 526) grid points. All model domains have 27 vertical layers, and the model top is set at 10 hPa. Model physics choices include the Kain–Fritsch cumulus scheme (Kain and Fritsch 1990, 1993), WRF single-moment six-class microphysics with graupel (Hong et al. 2004), and the Yonsei State University (YSU) scheme (Noh et al. 2003) for planetary boundary layer (PBL) processes. The cumulus scheme is not used on the innermost (3 km) grid. Radiative processes are calculated every 10 min on the 27-km grid and 5 min on the 9- and 3-km grids using the Rapid Radiative Transfer Model (RRTM) longwave (Mlawer et al. 1997) and Dudhia shortwave (Dudhia 1989) schemes. Finally,

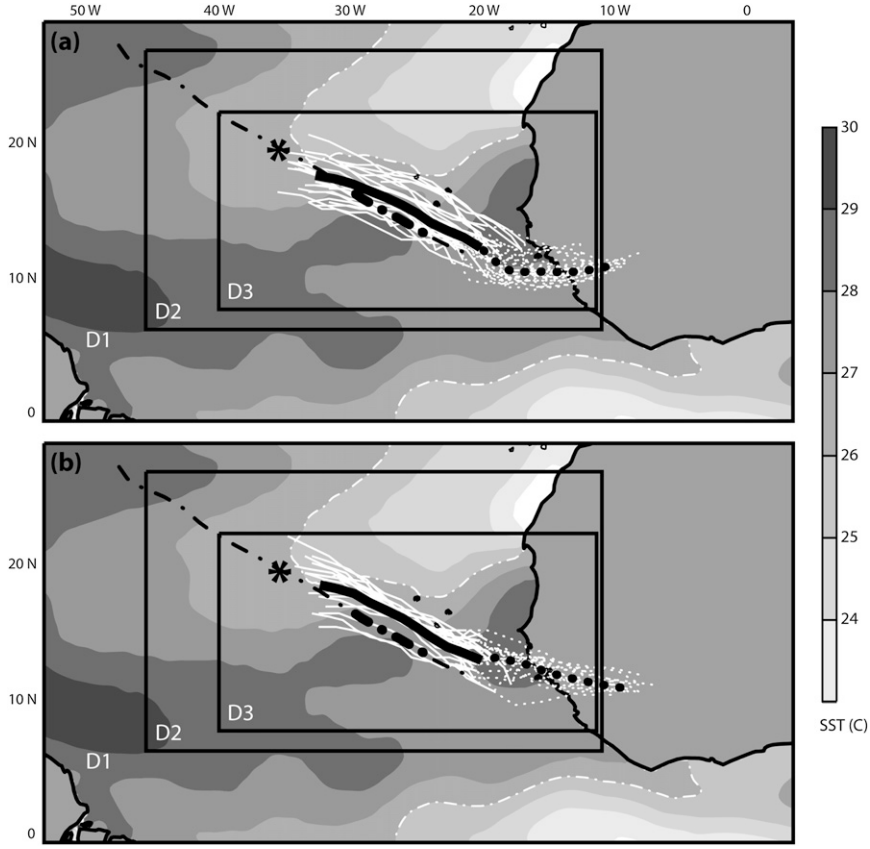

FIG. 4. The model domains (boxed), SSTs (shaded), and track of Debby for (a) CTRL and (b) WEAK. The dashed–dotted line represents the NHC postanalysis (the period of most intensification is thick), dotted lines are for the track of the large-scale 3-km PV anomaly at and before 36 h in the ensemble, and solid lines are for the track small-scale 1-km PV anomaly after 36 h. The thick black line represents the ensemble-mean track (calculated as the mean of the tracks in all the members), while the thin white lines represent the tracks in individual members. Ensemble tracks are plotted until 0600 UTC 24 August, while the entire observed track that fits within the domain is plotted with an asterisk denoting the position at 0600 UTC 24 August. The threshold of marginal SSTs (26°C) is denoted with a thin dashed–dotted line.

the impacts of aerosols (and therefore Saharan dust) are not investigated in this study.

SSTs are prescribed according to the FNL skin temperature (Fig. 4) and are not allowed to vary with time. The lack of ocean coupling may explain why some ensemble members, particularly in CTRL, forecast greater strengthening than observed in Fig. 5. Tropical cyclones have been observed to reduce SSTs by between 1° and 6°C (Black 1983; Bender et al. 1993) in their wakes, which could otherwise act to weaken a number of the stronger storms within these ensembles.

To create the CTRL ensemble random, but balanced, large-scale perturbations are added to 6-hourly 1° NCEP FNL analyses to create initial and boundary conditions for a 30-member ensemble of simulations. The initial time of the ensemble is 0000 UTC 20 August 2006, and it is integrated forward until 0000 UTC 25 August. This method, which is similar to that used in SZ08, implants noise derived from the NCEP background error statistics into the WRF three-dimensional variational data assimilation system (Barker et al. 2004). The initial rms ensemble spread varies with height from 1.3 to 2.3 m s^{-1} for zonal wind, 0.3 to 1.6 K for temperature, and 0 to 0.85 g kg^{-1} for mixing ratio and is comparable to rms differences between different global analyses (e.g., Fig. 1 of Zhang and Sippel 2009).

Although there has been some recent concern among both the general community and peer-reviewed literature that NCEP analyses do not properly capture the structure of the SAL (e.g., Pratt and Evans 2009; Reale and Lau 2010), we found the FNL analysis used for ensemble initialization here to be comparable in accuracy to the higher-resolution Modern Era Reanalysis (MERRA). For example, Fig. 6 compares the 0000 UTC 20 August

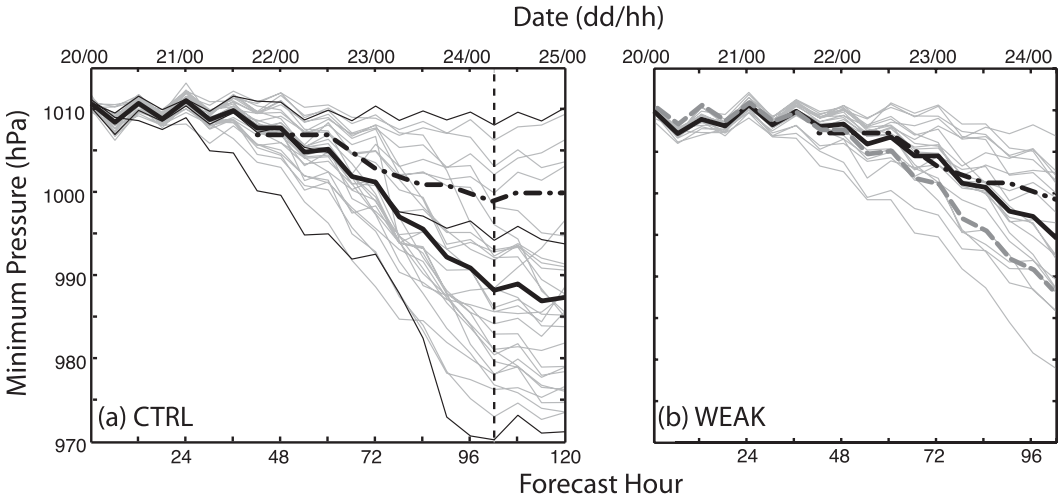

FIG. 5. Strength of Debby in terms of minimum SLP in (a) CTRL and (b) WEAK. The dashed–dotted line shows the strength of the observed storm according to the NHC postanalysis, the thin lines show the evolution of individual ensemble members, and the thick solid line shows the evolution of the ensemble mean (calculated as the mean of the minima in all members). The dark thin lines in (a) highlight storms in three members that are weak, moderate, and strong, and the vertical dashed line denotes the 102-h time in CTRL. The mean from (a) is also plotted in the gray dashed line in (b) for comparison between the two ensembles.

FNL analysis of layer-averaged specific humidity with that of MERRA and similar retrievals from the Atmospheric Infrared Radiance Sounder (AIRS). In the 850–700-hPa layer (Figs. 6a–c) FNL tends to be somewhat drier in the intertropical convergence zone (ITCZ) than either MERRA or AIRS observations, and the FNL ITCZ is somewhat broader so that the dry air is slightly farther from the incipient storm (nearing the African coast at this time). Meanwhile, MERRA is moister than AIRS above this level (Figs. 6d–i) so that FNL humidity is in better agreement with the AIRS data. Thus, *neither* analysis perfectly fits AIRS retrievals, which themselves inevitably contain some degree of error. Based on the above comparison and that of temperature data (not shown), the lower-resolution FNL does not seem to produce an inherently more inaccurate SAL analysis than does MERRA.

While it would be desirable to simulate the entire evolution of Debby, such a task is generally beyond the capability of the science given the length of the simulation required. Current operational forecasts extend only to 120 h because of large error at extended forecast times that is endemic to all current forecast models. The CTRL simulation in the current study also does not escape such error, as is apparent in Fig. 5a. While CTRL still spans Debby's strength at 120 h, the ensemble mean is at least 10 hPa too low starting around 96 h. A more serious concern for computing linear correlation is that cyclone strength in CTRL begins to exhibit bimodal behavior after about 102 h. Thus, the correlation analysis in CTRL will focus only on the time period from 0 to 102 h, and beyond that time only trajectories are analyzed to ascertain the source of dry air that wraps around the storm (see below).

To account for the possibility that the aforementioned intensity error in CTRL might shield the simulated storms from their environment (e.g., Reimer and Montgomery 2010, hereafter RM10) and result in unrepresentative correlation structures, we ran a sensitivity ensemble (WEAK) with weaker storms than in CTRL. The initial conditions for WEAK were created by perturbing the initial and boundary conditions of a weaker member in CTRL in the same manner as the FNL analyses were perturbed to create CTRL (a similar method was used to create an ensemble of weaker storms in SZ08). Because of the high computational cost of running an ensemble with such large domains, WEAK was limited to 20 members and integrated for only 102 h. Figure 5b shows that the ensemble mean in WEAK almost exactly matches Debby's intensity through 84 h, and the intensity error at 102 h is roughly half that in CTRL. For now, it is sufficient to say that storms CTRL and WEAK are related to their encompassing environment in somewhat different ways, although the impact of the SAL is similar.

b. *Wave and cyclone tracks*

These ensemble simulations cover the evolution from a larger-scale wave to the development of a mesoscale vortex, which complicates the determination of a single track in each ensemble member. There is no surface vortex during the earliest hours, so we initially track the 3-km PV anomaly associated with the disturbance that emerges off Africa. Because multiple mesoscale PV

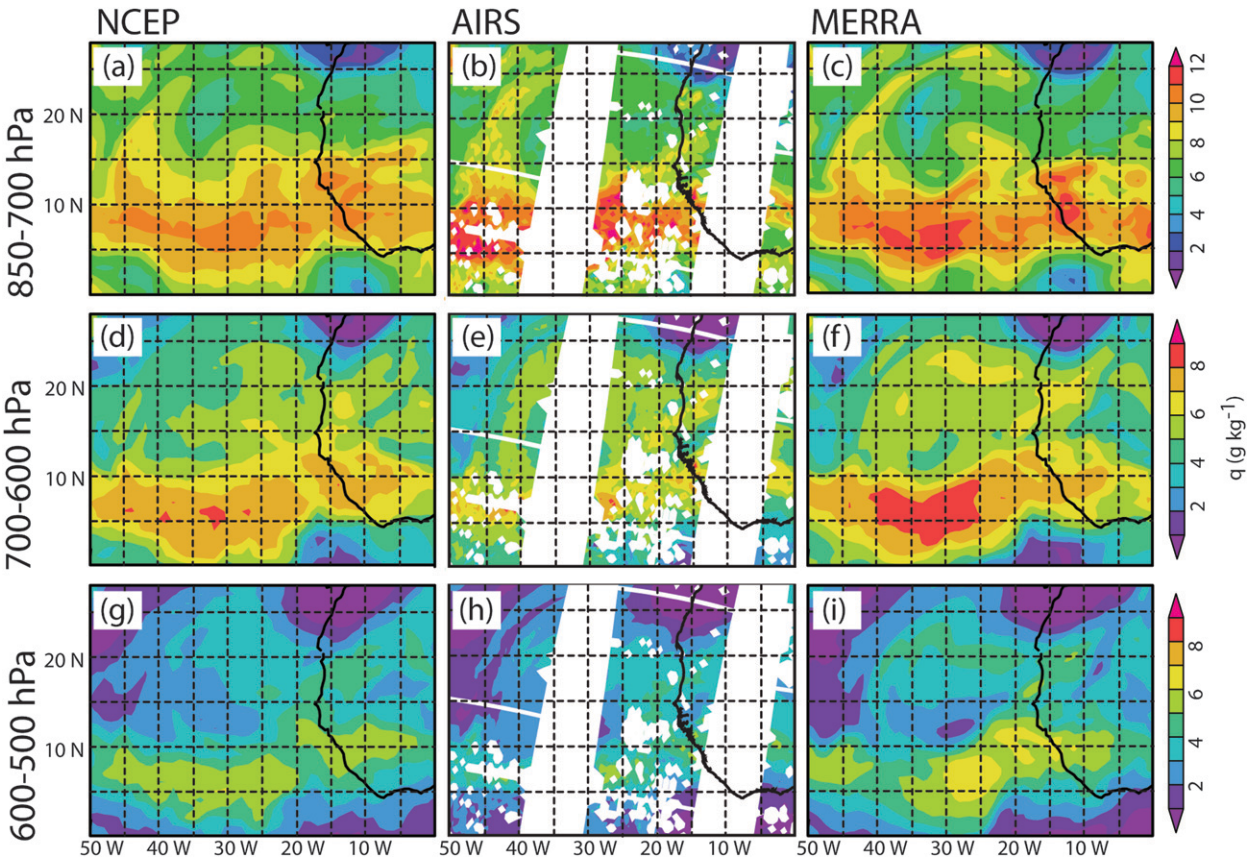

FIG. 6. A comparison of the (left) NCEP-FNL and (right) MERRA analyses with (middle) AIRS retrievals of layer-average relative humidity at 0000 UTC 20 Aug 2006.

anomalies form in many members, we first filter the PV field to remove scales less than 1000 km and then track the maximum of the filtered field as the center of the larger-scale vortex. By about 36 h, all members have a clearly defined surface circulation and PV tower, so the center position is thereafter assigned to be the location of maximum 1-km PV filtered to scales greater than 300 km. Using filtered PV to determine the cyclone track generally eliminates ambiguities posed by multiple smaller-scale circulation centers, particularly during the early period of genesis.

c. *Correlation analysis*

This study follows the framework of SZ08 and SZ10 by using linear correlation thresholds with magnitudes of 0.3, 0.5, and 0.7 and verbal descriptions of "weak," "moderate," and "strong." Confidence that a particular level of correlation is statistically different from 0 in CTRL is roughly 90%, 99.5%, and 99.99% for the respective thresholds, but it is slightly lower in WEAK owing to the use of fewer members (i.e., 80%, 95%, and 99%, respectively). To more easily facilitate comparison between WEAK and CTRL, a correlation of 0.38 in WEAK carries the same significance (90%) as 0.3 in CTRL. Likewise, a correlation of 0.36 in CTRL carries the same significance (95%) as does 0.5 in WEAK. While some might consider it desirable to show only regions where correlation is significant with greater than 95% confidence, we prefer our method because it more thoroughly shows the degree to which variance in one field explains variance in another. In particular, the given thresholds are convenient because they are associated with r-squared values of approximately 0.1, 0.25, and 0.5 (i.e., variance in one field respectively explains approximately 10%, 25%, and 50% of variance in another).

Although correlation can be used to compare ensemble behavior with physical reasoning developed in other studies (e.g., those mentioned in the introduction), it does carry caveats. First, it is well understood that correlation does not imply causality. Furthermore, the lack of linear correlation between two metrics simply means that they do not linearly vary with one another within the range of the ensemble. While this could imply that one does not affect the other, it is also possible that changes beyond what is spanned in the ensemble could yield different results or that the same two metrics could be nonlinearly related.

As in SZ10, this study makes frequent use of "part" correlation to clarify relationships when multiple variables are correlated to one another. To first order, it correlates two variables while effectively holding a third variable constant. For example, if variables x, y, and z are all correlated, then r_{yx} is the correlation between x and y, and $r_{y(x.z)}$ is the first-order part correlation between x and y with z held constant for x. Iterative equations are used for first- and second-order part correlations, respectively:

$$r_{y(x.z1)} = \frac{r_{yx} - r_{yz1}r_{xz1}}{\sqrt{1 - r_{xz1}^2}} \tag{1}$$

and

$$r_{y(x.z1z2)} = \frac{r_{y(x.z1)} - r_{y(z2.z1)}r_{x(z2.z1)}}{\sqrt{1 - r_{x(z2.z1)}^2}}. \tag{2}$$

For the dependent variable in Eqs. (1) and (2) (i.e., y), the strength of the mature cyclone is useful because it reveals the factors that might impact intensity in the ensemble. Similar to SZ08 and SZ10, here we define the intensity metric SLP_t, which is the negative of area-averaged sea level pressure, and the subscript t is replaced by a forecast hour. This metric at 102 h (0600 UTC 24 August), SLP_{102h}, is averaged within 50 km of the center and will be our mature cyclone intensity metric.

The strength controls used here, $z1$ and $z2$, are SLP_t (i.e., the above intensity metric) and average 1–3-km PV (hereafter referred to as $PVLL_t$, where t is again the forecast hour). This combination of strength controls more efficiently removes the signal of the wave and storm (at least for this particular case) than does the precipitation and PV combination used in SZ10. To calculate these controls, SLP and PV are averaged within a radius that decreases linearly with increasing forecast hour, from 500 km at 0 h to 50 km at 102 h. This change of averaging radius with time is a crude representation of the fact that the scale of a tropical cyclone is typically much smaller than that of a tropical wave. Results do not qualitatively change for different averaging radii.

Note that Eqs. (1) and (2) are slightly different than the corresponding equations in SZ10. That study analyzed the correlation between various predictors and a metric of future intensity wherein the future intensity metric was residualized. Thus, they investigated the relationship between total variability within each predictor and the *portion of future intensity variance* unexplained by their statistical controls. Meanwhile, Eqs. (1) and (2) show the relationship between *total variability in future intensity* and the portion of the predictor variance unrelated to current intensity. Using this slight alteration to SZ10, the square of a part-correlation value examined here is the part of *total intensity variance* uniquely related to the predictor (where uniqueness is in terms of the given controls). Correlation with the present set of equations is lower in CTRL after about 48 h and in WEAK after 72 h, wherein the SLP_{102h} residuals are weakly sensitive to a few environmental factors (using the SZ10 equations) but total variance in SLP_{102h} is insignificantly correlated with those same residualized factors (using the current equations). When sensitivity is lower using the present equations, the implication is that a given factor is either too weak to impact total SLP_{102h} variance or that it has not had sufficient time to significantly impact that variance. For example, SLP differences caused by variability in a given predictor at 48 h have much more time to grow than do differences caused by the same predictor at 84 h. Although the current set of equations carry the caveat of reducing correlation later in the ensembles, they have the benefit of explaining total SLP_{102h} variance as opposed to partial variance, which itself is a function of time and becomes a vanishingly small fraction of total variance near 102 h. Thus, the current equations more clearly quantify which factors uniquely relate to intensity variability and foster comparison between these factors at different times.

Whether a factor is too weak or has had insufficient time to impact total variance can be ascertained by comparing the evolution of correlation values for both sets of equations. If correlation is consistently significant with both but decreases to near 0 much more quickly with the current equations, then the factor being investigated likely continues to be important through the end of the simulation, but the intensity differences it induces become an increasingly smaller portion of total intensity variability. In situations where correlation is consistently insignificant with the current equations but significant with the SZ10 equations, the factor being investigated might only marginally impact simulated intensity. Significant differences are discussed when they occur, although only results using the current equation set will be shown.

d. Trajectory calculations

Backward trajectories[1] from select members of CTRL are calculated in section 6 in order to better understand the origin of dry air that wrapped around Debby on and after 23 August (Fig. 1e) and to at least subjectively understand the potential impact on the storm. To do this, the ensemble members of interest are rerun with

[1] Trajectories are calculated in terms of exponential height (z in meters) where vertical velocity is the time derivative of exponential height. Simulated horizontal and vertical motions are used to advance the trajectories backward in time.

15-min output on domain 1 (i.e., the 27-km grid), and RIP[2] version 4.3 is then used to linearly interpolate model output to 90-s intervals. The trajectories are released at every third grid point at 3 km. While it would be desirable to calculate trajectories for every ensemble member and run statistics, calculations from a few members are adequate for our needs in this study.

Trajectories are determined to be of potential SAL origin based on their initial position and relative humidity. First, a parcel must originate from within the boxed area of Fig. 1a (either at 0 h or along the lateral domain-1 boundary at some later time), which encompasses all of the high-AOD air in Fig. 3b. Although this box also includes a considerable amount of low-AOD air, using this simple guideline greatly simplifies the task. We next consider the typical altitude of the SAL, which Karyampudi and Carlson (1988) found to fall between 800 and 550 hPa just off the African coast. Thus, if a parcel's initial longitude is west of 17.5°W (essentially the African coast), then its initial altitude must fall between 1 and 6 km to be considered of SAL origin. Meanwhile, air over Africa (east of 17.5°W) must only originate below 6 km to be a candidate for SAL air. The depths used are a liberal interpretation of the 800–550-hPa depth, but we desire to err on the side of caution and place too many trajectories into the SAL category rather than too few (this proves to solidify our conclusions). Finally, any parcel that meets the aforementioned requirements must also have initial relative humidity less than 60% in order to be classified as dry SAL air.

4. Ensemble evolution and correlation analysis in CTRL

Using the part-correlation methodology described in section 3, this section investigates sources of 102-h intensity variance in CTRL. In particular, the nonaerosol impacts of the SAL are compared with other environmental influences.

a. Initial low-level PV

The factor most strongly related to cyclone strength at 102 h in CTRL is the strength of the initial PV anomaly that emerges off Africa. In the ensemble-mean 2-km PV and wind forecast shown in Fig. 7, this anomaly moves over the coastline on 20 August, intensifies as convection flares up off the coast, and becomes more symmetric in the wake of the large region of precipitation. Figure 8, which shows the evolution of correlation between $PVLL_t$ and SLP_{102h}, indicates that the 102-h storm intensity is moderately correlated to the mean low-level PV within and surrounding the initial large-scale PV maximum. Although the initial low-level PV magnitude here is prescribed according to WRF-VAR, this result suggests that any process that can increase low-level PV before a wave emerges off the coast can contribute to genesis. Such processes include organized convection (Haynes and McIntyre 1987; Raymond and Jiang 1990; Torn 2010) and both baroclinic and barotropic growth of AEWs (Thorncroft and Hoskins 1994).

These results are also reflected in the evolution of minimum SLP shown in Fig. 5, where the three black thin lines show minimum SLP for a few select members. By 12 h, the members with the lowest and highest SLP respectively remain the strongest and weakest members for most of the duration of the simulation. The remainder of this section discusses other environmental influences on Debby's genesis.

b. Atmospheric moisture

During the period of low-level vortex genesis, variability in nearby deep moisture appears to play a significant role in intensification rate of the simulated storm. To illustrate this in a mean sense, Fig. 9a shows the second-order part correlation between area-averaged mixing ratio and SLP_{102h} (controlling for SLP_t and $PVLL_t$) as a function of time and height.[3] During the first 6 h, the amount of water vapor through much of the troposphere above 2 km is weakly correlated with 102-h intensity. Thereafter, during the first 30 h of the simulation, SLP_{102h} is most consistently sensitive to moisture at altitudes from 2 to 4 km. The level of maximum sensitivity, where part correlation reaches a moderate value, occurs at 3 km. This is similar to the CTRL simulation of SZ08 for a Gulf of Mexico disturbance.

To better illustrate how the spatial distribution of moisture in CTRL is related to cyclogenesis, Fig. 10 shows maps of ensemble-mean 3-km mixing ratio and part correlation between mixing ratio and SLP_{102h}. After the first 6 h (Fig. 10a), regions of moderate positive correlation between SLP_{102h} and 3-km moisture are along the African coast just south of the PV center and within the moisture gradient to the northeast of the large-scale PV maximum (for clarity these regions are indicated with arrows). Thereafter, correlation near the coast south of the wave diminishes while that on the north side gradually transitions to an arch encircling the northern half of the 3-km circulation (Figs. 10c,e). There are also other regions

[2] Read–Interpolate–Plot software developed by Mark Stoelinga.

[3] When the independent variable in the correlation computation is an area average, the averaging area is computed similarly to that of SLP_t and $PVLL_t$ except that it decreases linearly with time from a 500-km radius to a 300-km radius. This approximately encompasses the precipitation shield of the wave and subsequent cyclone.

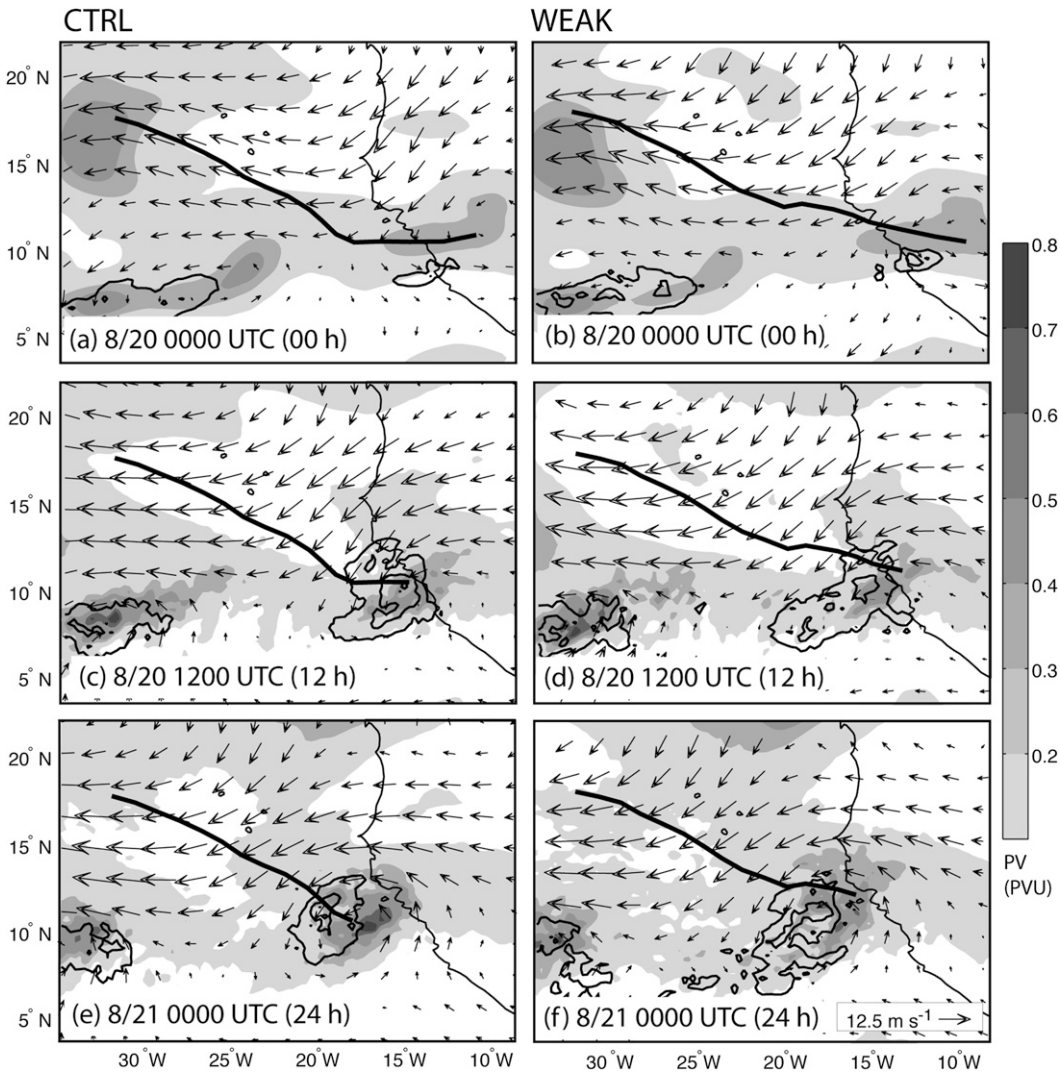

FIG. 7. A Lagrangian view of ensemble-mean 2-km winds and PV (shaded every 0.1 PVU) and 6-h rainfall (contoured every 15 mm) every 12 h from 0 to 24 h for (left) CTRL and (right) WEAK. The Lagrangian framework is composed by translating the subdomain of each member to the location of the mean position from Fig. 4.

of moderate correlation farther downstream of the wave, which most likely indicates sensitivity to the location and/or intensity of other weather systems. Hakim and Torn (2008) saw similar sensitivity patterns far from the feature that they were investigating and noted that the reason for their existence is not always clear, which is the case here as well.

The distribution of sensitivity to 3-km moisture near the wave in Fig. 10 implies that moisture variability in both the tropical air mass and the SAL transition region can affect genesis and intensification. For example, the weak to moderate sensitivity along the African coast in Fig. 10a (near 9°–10°N) occurs within an area of relatively high moisture in the tropical air mass. The second sensitivity region on the north side of the 3-km circulation in Fig. 10 roughly corresponds with the southern edge of the SAL according to AOD values (>0.2) in Fig. 3b (delineated with a white dashed line in Fig. 10e). This period of sensitivity begins before the disturbance moves offshore and ends as tropical depressions begin to form in many members.

Sensitivity to mean environmental moisture in Fig. 9 decreases considerably after 30 h, which suggests that the presence of nearby dry air during this period might not contribute to long-term strength variability. Moisture differences within the dry tongue that wraps around the west and south sides of the simulated cyclone in Fig. 11a are also unrelated to 102-h intensity variance. The moderate sensitivity to moisture during the first 30 h, but not at later times, is consistent with BSN11, who found that dry air above the boundary layer generally advects around but not into an established vortex. It is also consistent with

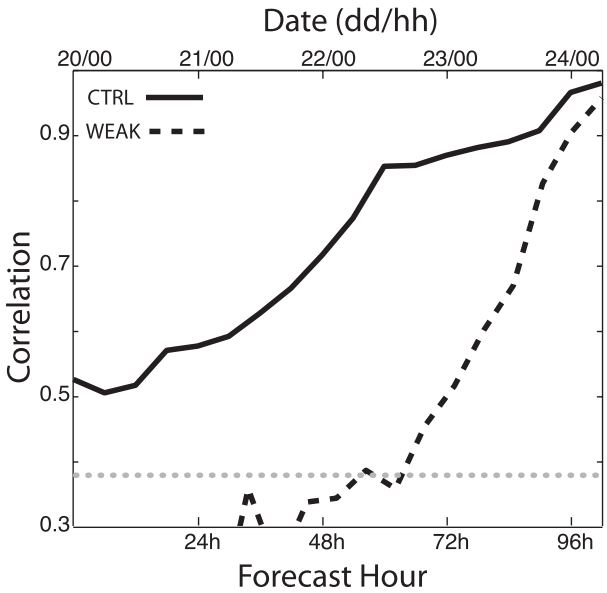

FIG. 8. The relationship between SLP_{102h} and $PVLL_t$ in CTRL and WEAK. $PVLL_t$ is calculated by taking an area average of 1–3-km PV within a distance from each member's center that decreases linearly with time from 500 km at 0 h to 50 km at 102 h. The change of averaging radius with time is a crude representation of the fact that the scale of a tropical cyclone is typically much smaller than that of a tropical wave. For comparison between the ensembles, correlation greater than that indicated by the horizontal dotted line is significant with >90% confidence.

RM10, who found that it is more difficult for external air to infiltrate a strong tropical cyclone than a weak one.

c. *Other potential factors*

We investigated the relationship between SLP_{102h} and a number of other factors, including area-average most unstable convective available potential energy[4] (MUCAPE), 2- and 3-km temperatures, the magnitude of deep-layer vertical wind shear,[5] and SST.[6] None is consistently related to SLP_{102h} variance in CTRL using Eqs. (1) and (2), although both shear and SST occasionally demonstrate periods of significant correlation using the SZ10 equations (not shown). With that set of equations deep shear demonstrates sporadic weak to moderate anticorrelation with the SLP_{102h} residuals between 48 and 78 h, and SST is weakly correlated to the residuals from 60 to 78 h. It must be emphasized, however, that these relationships are secondary to those between SLP_{102h} and both moisture and PV. The lack of a relationship between shear and intensity is not particularly surprising since deep-layer shear in CTRL is generally well below 5 m s^{-1}, which is low compared to the threshold of 12.5 m s^{-1} considered unfavorable by DeMaria et al. (2001) (shear through other layers is also relatively low). Somewhat more surprising is the lack of sensitivity to 2–3-km temperature, especially considering the apparent influence of dry SAL air within the same layer. Since cyclone intensity does not vary with 2–3-km temperature, it is possible that the lack of moisture within the southern extent of the SAL has a greater impact on intensification in these simulations than does its warm, stable layer. Finally, the result from SZ08 and SZ10 that high MUCAPE can hasten tropical cyclogenesis appears to not be true for this ensemble.

5. Sensitivity experiment WEAK

Spurred by concern that the erroneous strength of storms in CTRL could shield them from potentially negative influences of the outside environment, we constructed sensitivity experiment WEAK wherein cyclone strength more closely matches Debby's observed strength for the duration of the ensemble forecast. The correlation analysis here does yield somewhat different results, and the implication of the differences will be discussed here and in section 7. We must again caution the reader that confidence that a particular value of correlation is statistically different from 0 in this section is different than in the previous section. To facilitate comparison, regions of >0.38 (90% confidence) correlation, which corresponds to the significance of 0.3 in CTRL, are denoted in some figures.

a. *Initial low-level PV*

One of the biggest differences between CTRL and WEAK is in the correlation between initial low-level PV and 102-h intensity. Although the evolution of larger-scale PV in the two ensembles is initially quite similar in Fig. 7, Fig. 8 shows that the correlation between initial low-level PV and SLP_{102h} in WEAK is insignificant for at least the first 30–36 h. However, Fig. 12 shows that 6–12-h $PVLL_t$ (denoted $PVLL_{06h}$ and $PVLL_{12h}$) exhibits moderate to strong time-lag correlation with subsequent SLP_t for the first 48–60 h, and it falls to insignificant levels only in the later half of the simulation. In fact, time-lag correlation between $PVLL_{06h}$ and SLP_t is somewhat stronger in WEAK than in CTRL for a while, but it sharply falls after 36 h. Thus, initial low-level PV variability in WEAK is quite strongly related to subsequent differences in surface pressure, but these differences do not carry through with

[4] MUCAPE is computed as the CAPE for the parcel in each column with maximum equivalent potential temperature within the lowest 3000 m. Following the recommendation of Doswell and Rasmussen (1994), virtual potential temperature is used in this calculation.

[5] Shear is calculated as the vector difference between area-averaged winds in the 1–3- and 9–14-km layers. These layers roughly correspond to 700–925 hPa and 150–350 hPa, which DV04 recommended to adequately capture any effect of the AEJ.

[6] Although SSTs are not perturbed in these experiments, track variability over a region with an enhanced SST gradient (Fig. 4) results in storms that experience different SSTs.

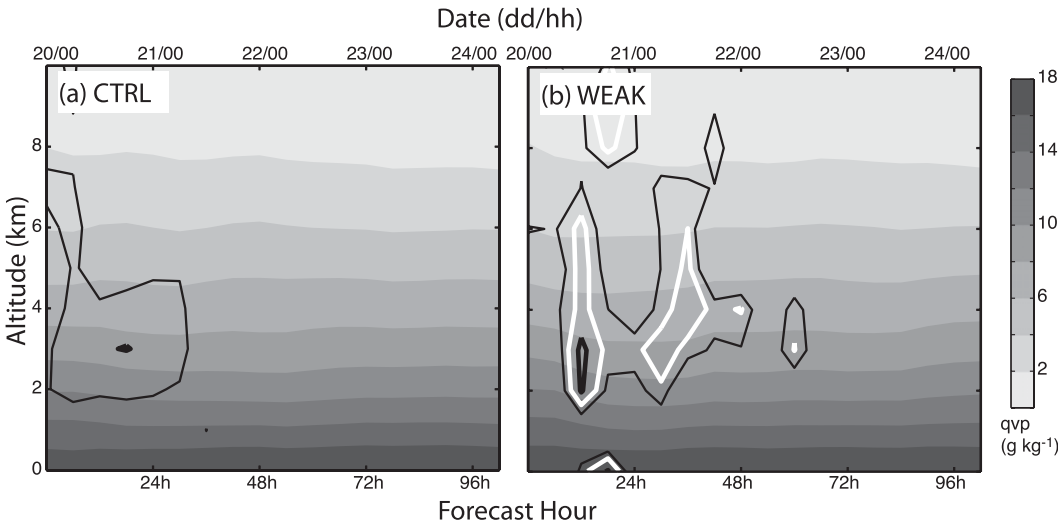

FIG. 9. Ensemble-mean area-average mixing ratio and its second-order part correlation with SLP_{102h} as a function of time and height in (a) CTRL and (b) WEAK. The mixing ratio is calculated by taking an average within a distance from each member's center that decreases linearly with time from 500 km at 0 h to 300 km at 102 h. This approximately covers the precipitation envelope in the ensemble. Mixing ratio is shaded every 2 g kg^{-1}, and correlation is contoured at 0.3, 0.5, and 0.7 (there is no significant negative correlation) with increasing magnitude of correlation indicated by increasing line thickness. For comparison with CTRL, the region of correlation in WEAK that is significant with >90% confidence is outlined in white.

time to the end of the simulation. This suggests that some intervening factor or factors begin to affect ensemble evolution in WEAK as early as 36 h and continue through much of the remainder of the simulation. The rest of this section examines those factors.

b. Atmospheric moisture

Sensitivity of 102-h intensity in WEAK to atmospheric moisture exhibits both similarities to and differences from that in CTRL. Figure 9b demonstrates that SLP_{102h} is significantly related to low- to midlevel atmospheric moisture for much of the first half of the simulation. Comparing Figs. 9a and 9b, the main difference between WEAK and CTRL is that moisture variability is related to 102-h intensity about 18–24 h longer in WEAK than in CTRL. Also, although correlation in Fig. 10 is considerably noisier[7] for WEAK, the spatial distribution of positive correlation near the strengthening cyclone is similar to that in CTRL.

Drier low–midlevel air in WEAK likely helps to delay organization within its members compared to those in CTRL. Although there is practically no difference in minimum SLP between the two ensembles for the first 48 h, considerable differences in vortex strength and structure do arise. For example, Fig. 13 shows that the mean PV tower at 48 h in CTRL is stronger and more symmetric, which likely helps cyclones in its members to intensify more quickly thereafter. Apparently slowing WEAK's organization up until this point is a pocket of dry air embedded in strong easterlies to the north of the center, which Figs. 10d and 10f show approaching from the northeast from 12 to 18 h. While air to the north of the PV maximum in CTRL also dries with time (Figs. 10c,e), it remains considerably moister than in WEAK. In addition, the mean system latitude in WEAK is somewhat farther north than CTRL at times during the first 36 h (e.g., Figs. 10e,f), which puts its cyclones closer to the environmental moisture gradient and dry SAL air.

Figure 14 shows differences in ensemble-mean 3-km mixing ratio between the two ensembles (WEAK − CTRL) and more visibly demonstrates the relatively dry air in WEAK from 18 to 36 h. For clarity, regions where the difference in means is significant with greater than 95% confidence according to the unequal variance *t* test are also highlighted. Air near the center of WEAK is consistently less than 0.5 g kg^{-1} drier than that in CTRL, and the

[7] The additional noise for WEAK in Fig. 10 is likely a result of a smaller sample size and the fact that moisture variability in WEAK is closely tied to the latitude of its individual members. Systems in WEAK that are farther north tend to be in drier environments, which is a leading cause for the signal in Fig. 9b. Adding the control of latitude completely eliminates the signal in Fig. 9b for WEAK, but not for Fig. 9a for CTRL (not shown). Because of this relationship with system latitude and the Lagrangian framework used, the correlation between cyclone strength and moisture is significant near enhanced meridional moisture gradients anywhere across the domain in WEAK (e.g., Fig. 10) whether or not moisture in those regions actually impacts intensity.

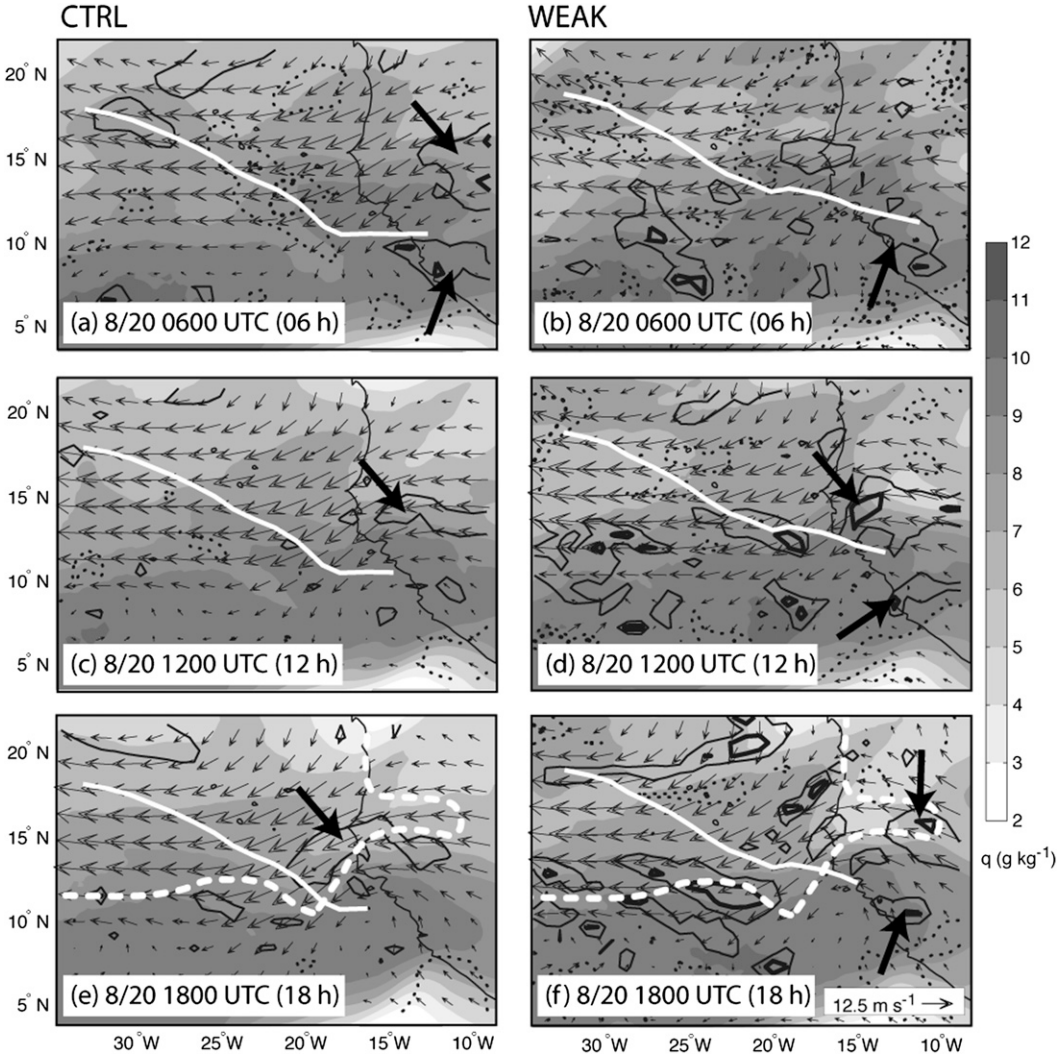

FIG. 10. A Lagrangian view of ensemble-mean 3-km mixing ratio (shaded every 1 g kg^{-1}), its second-order part correlation with SLP_{102h}, and ensemble-mean 3-km winds every 6 h from 6 to 18 h in (left) CTRL and (right) WEAK. The Lagrangian framework is composed as in Fig. 7, and correlation is contoured as in Fig. 9a with dashed lines for negative correlation. The white solid line represents the track of the ensemble mean, as in Fig. 4, and the thick arrows point to areas of positive correlation near the wave and developing cyclone that are referenced in text. The white dashed line in (e) and (f) corresponds to where AOD > 0.2 in Fig. 3b.

moisture deficit increases to over 2 g kg^{-1} about 350 km north of the center at 18 h. The region of greatest deficit is congruent with the location of the dry tongue generally north of WEAK's mean center in Fig. 9f, and it translates from northwest to west of the center by 36 h within the background cyclonic flow. The effect of latitudinal differences between the two ensembles can also be seen in Fig. 14. This signal is strongest at 18 h when there is a noticeable dipole in difference values (e.g., in Fig. 14a there is a moisture deficit to the north and surplus to the south). Although air to the south in WEAK is relatively moist compared to that in CTRL due to this effect, the regions of statistically significant difference here are relatively far from the center.

The results of WEAK seem to support the idea that weaker storms are less able to shield themselves from a harsh environment. For example, storms in WEAK have a weaker, more asymmetric low-level PV anomaly through 48 h (Fig. 13), which could help to explain the temporally longer sensitivity to moisture. Nevertheless, correlation between moisture and 102-h intensity eventually decreases despite the continued presence of dry air. In addition, moisture differences within the dry tongue that later wraps around the center again are unrelated to variability in intensification (Fig. 11b). This behavior is quite similar to that of CTRL and is consistent with BSN11 and RM10.

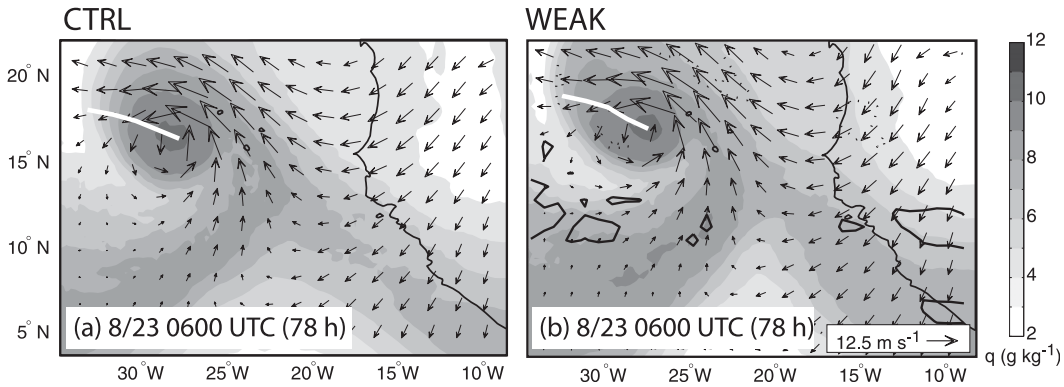

FIG. 11. As in Fig. 10, but for 78 h.

c. *Sea surface temperature*

Perhaps the biggest difference between the two ensembles is in sensitivity to track-related SST variance. While SST differences are generally unrelated to total SLP_{102h} variance in CTRL, Fig. 15 shows that part correlation between the two variables (bold solid line) in WEAK is significant from 48 to 78 h. In fact, track-relative SST in WEAK eclipses moisture as the strongest predictor of 102-h intensity. Furthermore, using the SZ10 equations, correlation between SST and SLP_{102h} residuals remains around 0.6 through 84 h and only becomes insignificant at 96 h. This reveals that SST likely continues to impact cyclone intensity past 78 h, but SST differences beyond this point do not have sufficient time to impact total SLP_{102h} variance. Since storm tracks are slightly farther north in WEAK (Fig. 4), average SST along the mean track is up to 0.3 K cooler than in CTRL during this time period. This small but persistent difference likely contributes to the lower intensification rate in WEAK.

There are several potential reasons for the difference between CTRL and WEAK in sensitivity to SST. First, initial spread grows much more quickly in CTRL, which might mask later SST-induced strength differences. Thus, the significant part correlation between SST and SLP_{102h} using the SZ08 equations could suggest that SST-induced differences simply have insufficient time to grow into a meaningful portion of the much larger intensity spread in CTRL. Furthermore, storms in WEAK experience greater SST variance during the time of significant correlation (not shown), which might be inducing stronger differences between its ensemble members. Finally, differences in SST between the members of WEAK are more temporally consistent than those in CTRL. For example, Fig. 16 shows the time-lag correlation between 48-h, 54-h, and 60-h SST (denoted SST_{48h}, etc.) and subsequent SST_t through 78 h. Storms experiencing cooler SST in WEAK from 48 to 60 h have a much stronger tendency to continue to experience cooler waters along their tracks through 78 h. This temporal consistency likely allows even small SST differences between individual members to translate into incrementally larger strength differences within WEAK.

d. *2–3-km temperature*

The temperature of air near the bottom of the Saharan air layer might also impact intensification during the first 42 h of WEAKs evolution, but its relationship with intensity variance is not strong. Figure 15, which shows the second-order part correlation between SLP_{102h} and area-average 2-km temperature (denoted $T2KM_t$), demonstrates an occasional weak relationship between temperature and storm intensity that is concomitant

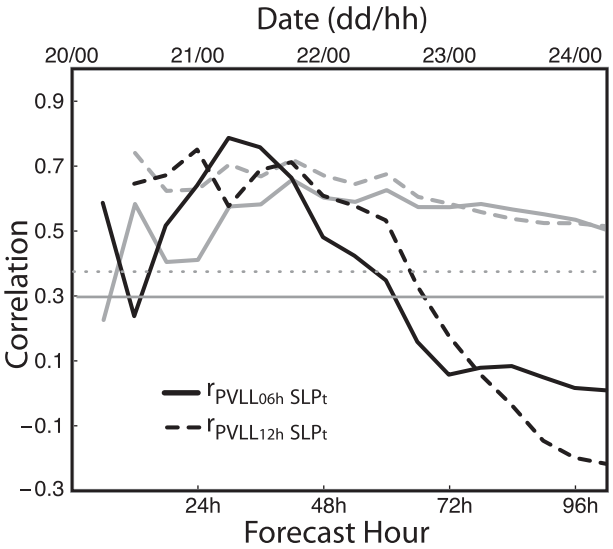

FIG. 12. Correlation between the initial PVLL and subsequent SLP_t in WEAK (black) and CTRL (gray). The relationship for $PVLL_{06h}$ is shown with a solid line, and that for $PVLL_{12h}$ is shown with a dashed line. Correlation greater than that indicated by the horizontal dotted (solid) line is significant with >90% confidence in WEAK (CTRL). Area averages are calculated as in Fig. 8.

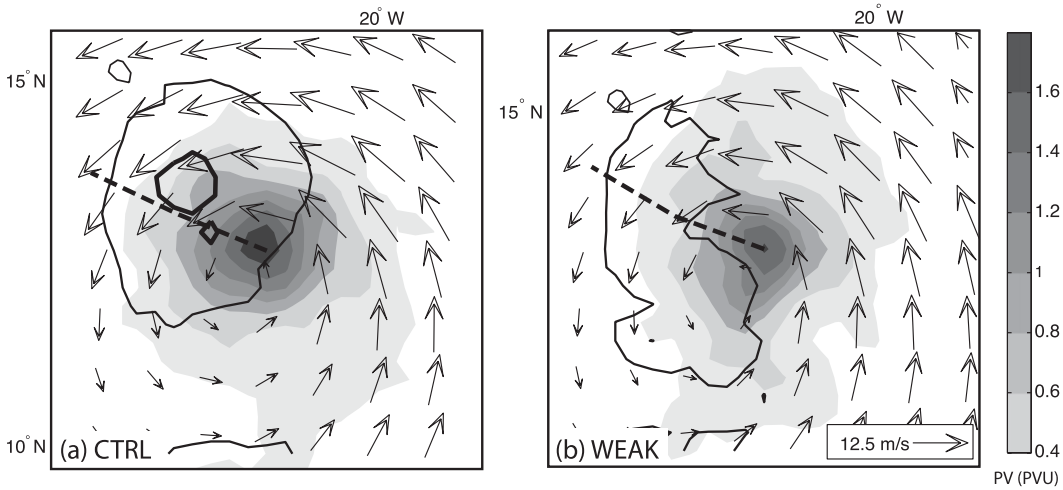

FIG. 13. A zoomed-in view of ensemble-mean PV and winds at 2 km and 6-h subsequent precipitation in (a) CTRL and (b) WEAK at 48 h. Potential vorticity is shaded every 0.2 PVU, 6-h precipitation is contoured every 15 mm, and the mean track is plotted with a dashed line. The Lagrangian domain is composed as in Fig. 7, except that the storm center is at the center of each panel.

with sensitivity to low- to midlevel moisture. The relationship is stronger at 2 km than at other levels within the SAL, so to the degree that a warm inversion layer does inhibit intensification in WEAK, it is likely because of temperature at this low level. Nevertheless, the correlation only exceeds the 90% confidence level once during the first 42 h and, viewed in that respect, the correlation here is generally similar to that observed in CTRL.

The stronger sensitivity to 2-km temperature after 42 h appears to be a result of the relationship between SST and SLP_{102h}. The background SST gradient is oriented similarly to the 2-km temperature gradient, so to the extent that temperature variability depends on track, differences in SST also correspond to 2-km temperature differences. To separate these two factors, Fig. 15 also shows the third-order part correlation between 2-km temperature (SST) and SLP102h wherein SST (2-km temperature) has been added to PV_t and SLP_t as a statistical control. Including SST as a statistical control in the part correlation between SLP_{102h} and 2-km temperature reduces the correlation to near 0 starting around 48 h, which is when the second-order part correlation between SST and SLP102h increases to significant levels. Meanwhile, including 2-km temperature as a control in the second-order part correlation between SST and SLP_{102h} only slightly reduces that correlation. This strongly suggests that the main reason for significant correlation between 2-km temperature and SLP_{102h} after 42 h is the sensitivity to SST.

e. Other potential factors

As in the previous section, we investigated the relationship between SLP_{102h} and both area-average MUCAPE and the magnitude of deep-layer vertical wind shear. Similar to CTRL, using Eqs. (1) and (2) reveals no relationship between shear differences and total SLP_{102h} variance, but the SZ10 equations show *sporadic* weak to moderate correlation between 72-h and 96-h shear and the SLP_{102h} residuals (not shown). Thus, shear could be affecting intensity in WEAK during this time period, but its overall relationship with intensity variance is strongly secondary to that of SST and moisture variability. Since shear values generally remain well below 5 m s^{-1} in WEAK, which is again in a favorable range for TC intensification, this weak relationship is not unexpected. Finally, variability in MUCAPE is unrelated to intensification in WEAK.

6. Trajectory analysis

This section investigates the source and potential impacts of the dry air that wraps around the western and southern sides of the observed (Fig. 1e) and simulated (Fig. 11) cyclones. Although we chose not to investigate the correlation relationships beyond 96 h, the analysis here uses back trajectories to show how the dry slot forms, evolves, and varies with storm intensity. Figures 17–19 show trajectory data from three ensemble members that span CTRL in terms of cyclone strength at 72, 96, and 120 h. The storm in member 8, with a minimum SLP consistently above 1008 hPa, is the weakest of the three. Meanwhile, the member-14 cyclone strengthens from about 1009 to 991 hPa, and that in member 20 strengthens from about 1000 to 975 hPa during this time period. For all three members in Figs. 17–19, 3-km air at

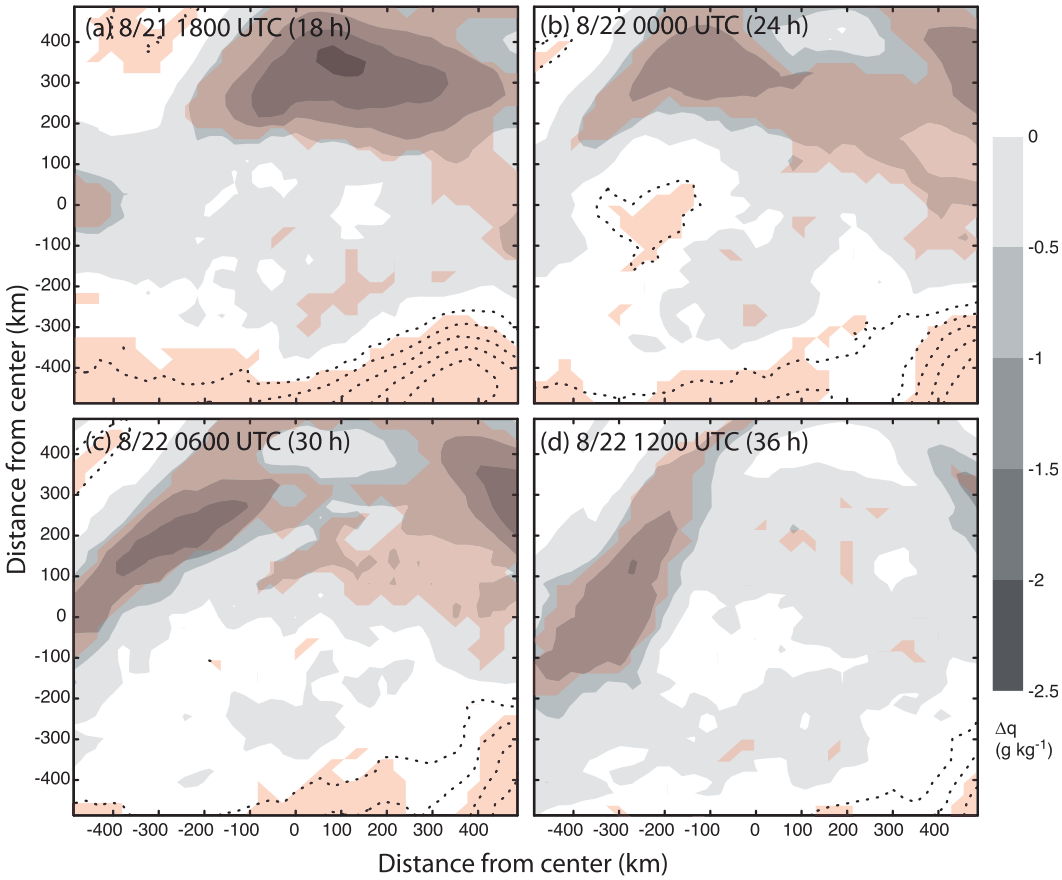

FIG. 14. Difference in the ensemble-mean 3-km mixing ratio between WEAK and CTRL (WEAK − CTRL) every 6 h from 18 to 36 h. Negative values are shaded and positive values are contoured every 0.5 g kg^{-1}. Regions where the difference in means is significant with >95% confidence according to the unequal variance *t* test are shaded in translucent red. The center of each panel corresponds to the mean position in each ensemble so that these differences are computed in a storm-centered framework.

the given time is determined to be of potential SAL origin according to the method described in section 3d. Recall that calculations are performed for every third grid point on domain 1, which has 27-km grid spacing. If this air has a history within the SAL, then it is shaded in gray and overlaid upon the relative humidity field in the left columns and upon the net vertical displacement in the right columns. The net vertical displacement *dz* in these figures is the difference in altitude between the time of release of the trajectories (i.e., 3 km at 72, 96, or 120 h) and the model initial time. In the case that the trajectory originates from a lateral boundary after the model start time, the vertical displacement is calculated using the height at the time that the trajectory enters the domain.

The back trajectories reveal that much of the 3-km air in the dry slot is not of Saharan air layer origin, even when potential SAL air surrounds simulated storms through 120 h. For example, the continuously weak storm in member 8 is almost completely surrounded by SAL air at 72 h as a pronounced dry tongue begins to form within non-Saharan air just west of the leading edge of the SAL (Fig. 17a). Non-SAL air gradually deforms and replaces the SAL air mass so that the only potential SAL air within the dry slot from 96 to 120 h is on its eastern and southern edges (Figs. 18a and 19a). The moderately intensifying storm in member 14 has a fairly large region of potential SAL air in its dry slot at 96 h (Fig. 18c) and, while plenty of potential SAL air remains at 120 h, it has been displaced radially outward from the center by dry non-SAL air (Fig. 19c). Thus, non-Saharan air is generally closer to the center and dryer than Saharan air in the member-14 dry tongue by 120 h. A similar pattern is noted for the dry slot of the most rapidly intensifying storm in member 20 (Fig. 17e), where the driest air closest to the center is not of SAL origin by 120 h (Fig. 19e). While these results imply that there might have been SAL air within Debby's dry slot, this air would have been generally farther from the storm than the driest, non-SAL air.

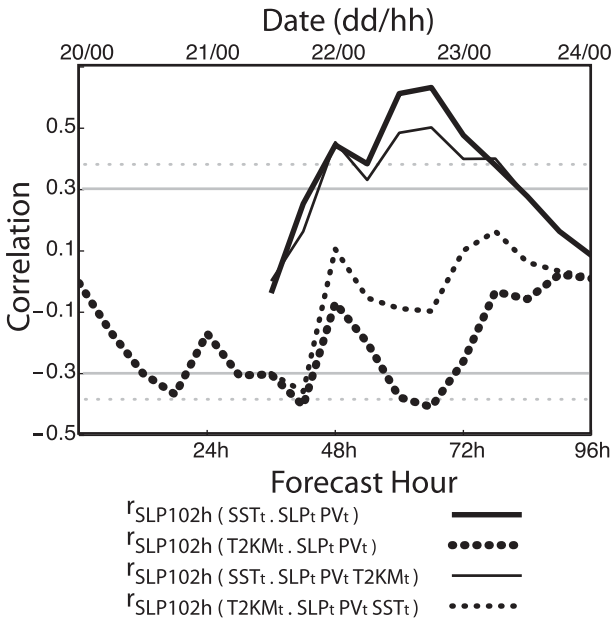

FIG. 15. The relationship among area-average SST (SST_t), 2-km temperature ($T2KM_t$), and SLP_{102h} in WEAK. The evolution of second-order part correlation between SLP_{102h} and area-average SST ($T2KM_t$) is shown with a thick solid (dotted) line. The third-order part correlation between SST_t ($T2KM_t$) and SLP_{102h}, adding the additional control of $T2KM_t$ (SST_t), is shown with a thin solid (dotted) line. The relationships involving SST are only shown after 36 h since the calculation at earlier times is strongly contaminated by skin temperature over land. Area averages are calculated as in Fig. 9. Correlation with a magnitude greater than that indicated by the horizontal dotted (solid) line is significant with >90% confidence in WEAK (CTRL).

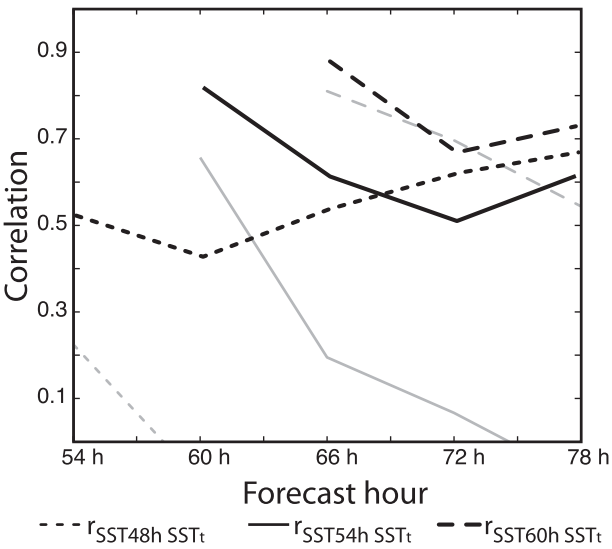

FIG. 16. Time-lag correlation between the area-average SST at 48 (dotted), 54 (solid), and 60 h (dashed) and subsequent SST in WEAK (black) and CTRL (gray). Area averages are calculated as in Fig. 9.

The trajectories also reveal that the driest air surrounding the simulated storms often has a history of strong subsidence. This finding is true for all three members shown at all times but is most pronounced in member 20, where trajectories with over 3 km of net subsidence encircle the strengthening cyclone by 120 h (Fig. 19e). In addition, there are a number of times when air of African origin has a history of subsidence. For example, potential SAL air around the cyclone center in member 20 from 72 to 120 h (Figs. 17–19f), southwest of the center in member 8 at 96 h (Fig. 18b), and west to southwest of the center in member 14 at 96 to 120 h (Figs. 17–19d), has subsided around 2 km. In this circumstance, the initial amount of moisture in the air may be much less important than the drying effects of subsidence.

Regardless of airmass origin, these figures reiterate that the mere presence of dry air around a tropical cyclone does not necessarily mean that the cyclone will weaken. For example, member 20 has the driest air with relative humidity near 20% wrapping to within several hundred kilometers of the center, during which time it strengthens by 25 hPa. In fact, Fig. 19 suggests that relative humidity in the dry slot varies negatively with cyclone intensity, likely because stronger storms are surrounded by air with a history of stronger subsidence. This is consistent with knowledge of the tropical cyclone secondary circulation and demonstrates that care must be used when attempting to interpret the effects of dry air, particularly for mature cyclones.

7. Discussion and conclusions

This study has used WRF ensemble forecasts to compare the nonaerosol impacts of the SAL to other environmental influences on the intensity of Tropical Storm Debby. Debby formed from an AEW just off the African coast but never intensified beyond a moderate tropical storm. To examine the influences on intensification, similar methodology to that of SZ08 and SZ10 is used to investigate why storms in some ensemble members rapidly form a hurricane and others do not. In particular, we examine part correlation between various fields and 102-h SLP to better understand the factors that affected Debby's intensification. This is the first time that an ensemble has been used to quantify the influence of the SAL on tropical cyclone development.

The CTRL ensemble, whose initial conditions were created by perturbing an NCEP-FNL analysis, produces a set of tropical cyclones that spans Debby's strength and track, albeit with considerable mean intensity error. Minimum SLP at 102 h in CTRL ranges from about 970 to 1010 hPa, and about 20% of the ensemble storms remain at or below Debby's observed intensity at that

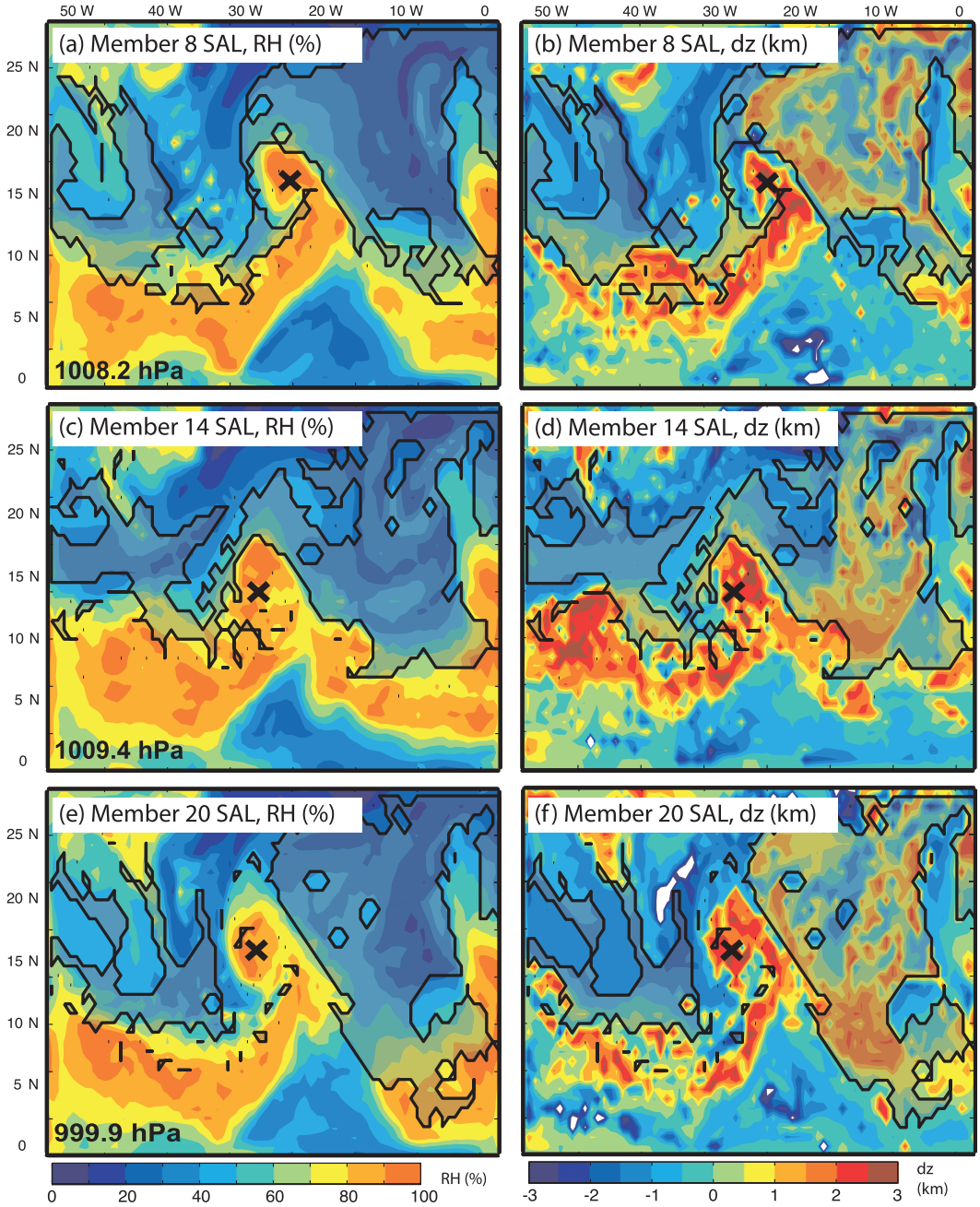

FIG. 17. The relationship among the Saharan air layer, atmospheric moisture, and subsidence for select ensemble members at 72 h. (left) Relative humidity at 3 km is color-filled every 10%, and (right) net vertical displacement for back trajectories released from 3 km is color filled every 0.5 km from −3.0 (i.e., net subsidence) to 3.0 km (i.e., net ascent). Potential SAL air is shaded darker, and the boldface san serif X denotes the center position in each member. The minimum SLP is shown in the lower left-hand corner of the relative humidity panels.

time. The ensemble mean is about 10 hPa too low, which provides motivation for the creation of a second ensemble with weaker storms (see below).

The two factors in CTRL found to most strongly relate to 102-h cyclone intensity are the strength of the initial low-level PV disturbance and the amount of moisture encompassing the disturbance during the first 24–30 h of integration. Time-lag correlation between 102-h SLP and initial low-level PV surrounding the disturbance is between 0.5 and 0.6, which means that initial low-level PV differences explain about 25%–35% of 102-h intensity variability. The correlation begins

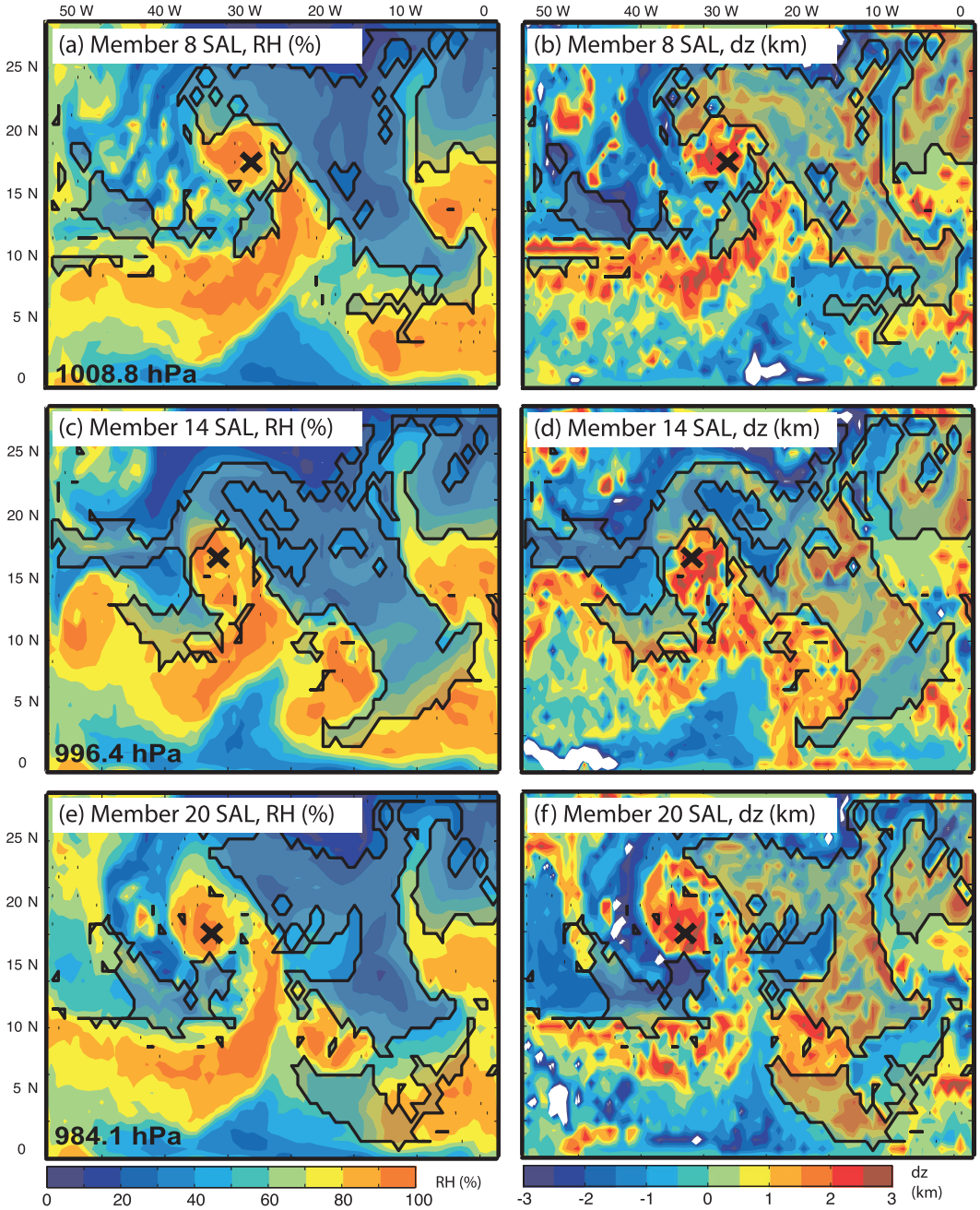

FIG. 18. As in Fig. 17, but for 96 h.

while the disturbance is over Africa, which suggests that processes that increase low-level PV over the continent (i.e., baroclinic or barotropic AEJ instability or organized convection) can hasten cyclone genesis and intensification once a disturbance moves over the ocean. In effect, since both PV and SLP are metrics of vortex strength, this moderate correlation means that vortices that start out the strongest tend to stay the strongest, though on a smaller scale. In addition, part correlation between 102-h intensity and average mixing ratio surrounding the disturbance briefly peaks at about 0.5, which means that moisture variance explains up to an additional 25% of intensity variance. Further investigation reveals that the relationship between moisture and cyclone intensity is due to moisture variability within both the ambient tropical air mass and the southern portion of the Saharan air layer, which extends to the edge of the developing disturbance. The relationship between moisture and storm intensity is

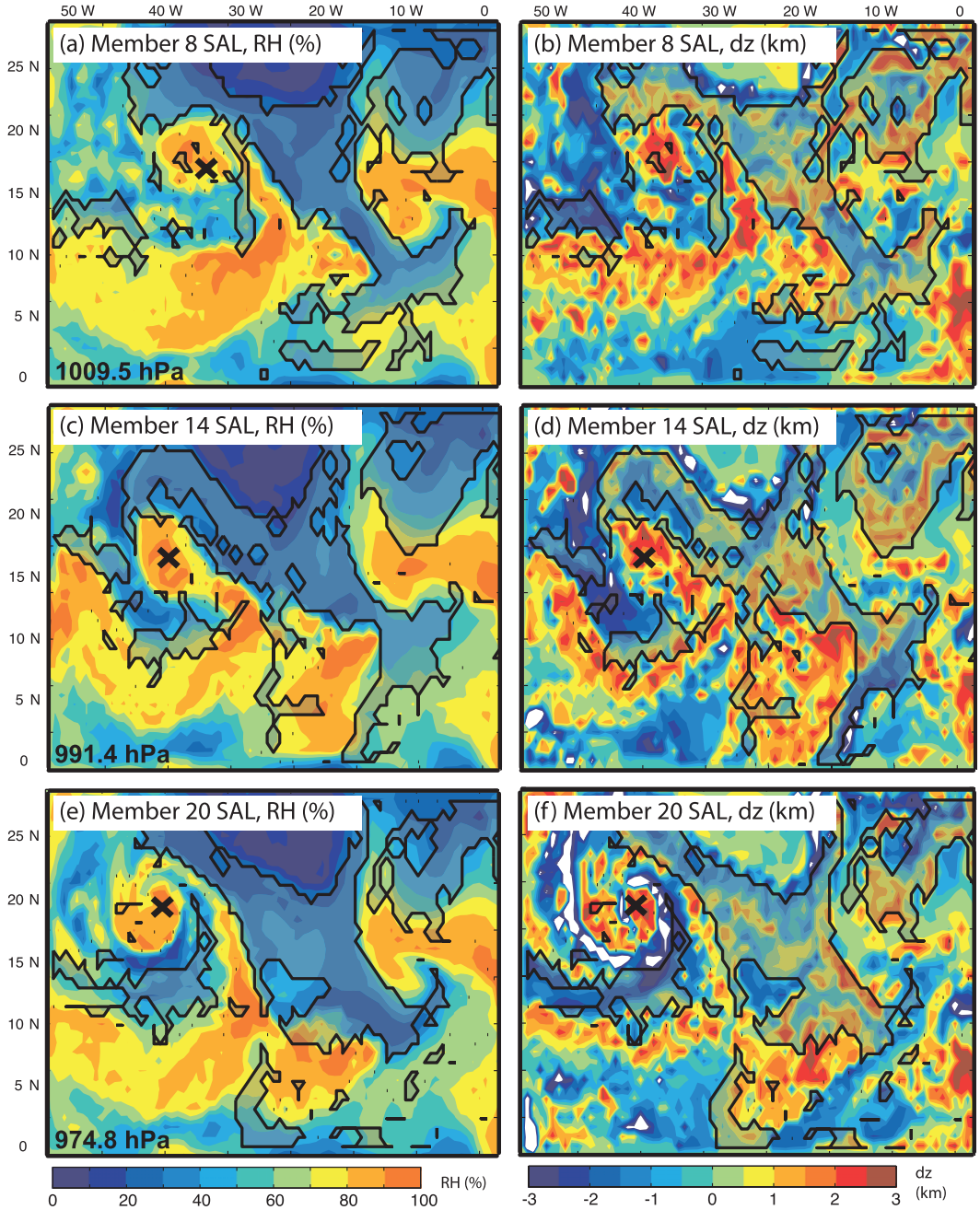

FIG. 19. As in Fig. 17, but for 120 h.

limited to the first 24–30 h, during the predepression to early depression stages, and the presence of nearby dry air later on is unrelated to subsequent changes in storm strength. Other potential factors related to the SAL, including 2-km and 3-km temperature and (generally weak) vertical wind shear, have at most a weak secondary relationship with intensity variance in CTRL.

Spurred by concern that the erroneous strength of storms in CTRL essentially shields them from potentially negative influences of the outside environment, we constructed sensitivity experiment WEAK wherein ensemble-mean cyclone strength more closely matches Debby's observed strength for the duration of the ensemble forecast. The initial conditions for WEAK were created by adding perturbations to a weaker member of CTRL in a manner similar to the way that NCEP-FNL analyses were perturbed to create the CTRL initial conditions. This method is similar to that used in SZ08,

and the reduction in intensity error is about 50% after 102 h.

Environmental conditions related to 102-h intensity in WEAK exhibit both similarities to and differences with those in CTRL. In this case, the factors most strongly correlated with storm strength at the end of the simulation are SST and moisture above 2 km. Part correlation between 102-h SLP and 3-km moisture peaks just above 0.5, which is similar to the peak value seen in CTRL, but the relationship continues about 18–24 h longer than in CTRL. Meanwhile, a major difference from CTRL develops after 48 h when the relationship between SST and cyclone intensity becomes significant. Part correlation between SST and 102-h SLP increases to nearly 0.65 at 66 h, which explains about 40% of 102-h intensity variance, and remains significant until 78 h. Further investigation reveals that SST differences likely continue to impact intensity through 96 h, but they do not have sufficient time to significantly impact total variability in 102-h intensity. There is also a weak relationship between storm strength and 2-km temperature early in WEAK, which likely represents very weak sensitivity to the stable layer at the bottom of the SAL. Nevertheless, the correlation is significant with greater than 90% confidence only once and, in that respect, is similar to CTRL. Also as in CTRL, the weak vertical wind shear present in the ensemble exhibits a weak secondary relationship with SLP. Finally, the other major difference between WEAK and CTRL is that variability in the strength of WEAK's initial PV anomaly is unrelated to the 102-h storm strength.

The major differences between the two ensembles in terms of SST and PV correlation can be explained by further investigation and give insight into cyclone behavior. With regard to PV, in WEAK there is significant time-lag correlation between initial PV and subsequent SLP for the first 48–60 h of the simulation, but the correlation is annihilated by the long duration of sensitivity to water vapor and the relatively strong sensitivity to SST. In effect, the strongest systems at 30 h in WEAK are not necessarily strongest at 60–72 h because of the intervening factors of moisture and SST variability. Thus, the strength of a low-level PV disturbance over Africa *can affect* how quickly the subsequent cyclone develops, but a stronger initial disturbance does not necessarily guarantee long-term viability of the cyclone. This is similar to the results of Torn (2010), who found in ensemble forecasts of an AEW that memory of initial AEW strength decreased in time as sensitivity to midlevel equivalent potential temperature increased. Meanwhile, WEAK's enhanced sensitivity to SST appears to be a result of its lower 102-h SLP spread and its stronger temporal consistency in track-relative SST variations. There is some suggestion that SST-induced intensity differences in CTRL may have insufficient time to grow into a significant portion of its large spread. In addition, storms experiencing lower SSTs at 48–60 h in WEAK continue to do so through 78 h, which has an incrementally larger effect on intensity. Thus, time-integrated SST changes are more relevant to long-term intensity trends than are short-term SST differences. This appears to be consistent with the results of Davis and Bosart (2002), Davis et al. (2008), and Bender and Ginis (2000).

Another important result of this study is the suggestion that sensitivity to encompassing environmental moisture depends on cyclone strength. The relationship between low to midlevel moisture and 102-h SLP in both ensembles is strongest during the predepression phase, while the disturbance is still over the African continent and nearing the coast. The correlation generally weakens with time as the system moves over water and the low-level vortex strengthens, and it decreases to insignificant levels at or before the middepression phase. Given the above tendency, it appears that the most vulnerable stage for entrainment of unfavorable environmental air is very early during the life cycle of a tropical cyclone. This strength-dependent relationship might also explain the longer period of sensitivity to moisture in WEAK, which has a weaker and less symmetric 2-km vortex after 48 h than does CTRL. Later, even as dry air wraps around the western and southern sides of the storm and to within 250 km of the cyclone center in both ensembles, there is no relationship between intensification and moisture in the dry tongue. In fact, extended analysis of a few members of CTRL to 120 h reveals that the driest 3-km air surrounds the *strongest* storms. Thus, extreme caution should be used when attempting to interpret the effect of this dry air on storm evolution for more mature cyclones. These results are in conceptual agreement with RM10, whose work also suggests that stronger storms are less susceptible to entrainment of dry air. They are also similar to BSN11, who found that dry air had only a delaying effect on development when it began at a very close radius (inside ~200 km) to the vortex center in idealized simulations.

The above results clarify the effects of the SAL on Debby relative to other environmental influences. In particular, the most likely impact of the SAL on Debby's intensity was dry air that slowed development of the system during the predepression to early depression stages. Keeping in mind the caveats associated with ensemble correlation, the lack of sensitivity to warm air within the SAL and AEJ-related shear suggest that they only weakly impacted Debby through early 24 August. Curiously, Debby's most rapid intensification began roughly when sensitivity to average environmental

moisture in WEAK ended, which could indicate either that the spurt of observed intensification was a reflection of Debby's emergence from the influence of dry SAL air or that the dry SAL air became ineffective at retarding growth upon the initiation of well-organized deep convection in the moist tropical air mass. The increase in sensitivity to SST in WEAK also corresponds with Debby's observed intensification over warmer water, which implies that SST changes did impact the storm's intensity. Just as Debby's track over warmer SSTs on 22–23 August appears to have helped the storm intensify, the storm's failure to continue intensifying on 23–24 August was likely a result of movement over lower, more marginal SSTs.

Although we do not perform correlation analysis beyond 96 h and thus cannot statistically assess what ultimately caused Debby to weaken, the results of the trajectory analysis here combined with observations in section 2 and other recent research give considerable insight into what may have led to Debby's demise. Observational evidence shows that the most likely cause for Debby's dissipation was a dramatic increase in vertical wind shear associated with an upper-level trough from 24 to 26 August (Figs. 1f,h). RM10 found that increasing shear tends to help environmental air infiltrate closer to the center of a TC, so it is conceivable that the higher shear that Debby encountered after 24 August could also have entrained air from the observed dry tongue. However, even if the dry tongue hindered Debby's intensification after 96 h, back trajectories reveal that blame cannot generally be placed on the SAL. Although some air within the dry tongue evidently had SAL origins, the back trajectories here reveal that much of the driest air was likely from outside the SAL and had a strong history of subsidence.

While this study has the limitation of only investigating one system, we believe that these results carry some degree of generality. For example, our conceptual congruence with the idealized work in RM10 demonstrates that intensity-dependent sensitivity to the environment is not limited to Debby. Furthermore, our finding that much of the air in the dry tongue is of non-SAL origin strongly agrees with the similar assessments of Braun (2010a). Thus, this study reiterates the point raised by Braun that proximity of the SAL does not imply a negative influence on the intensity of a storm. While the sensitivity to AEJ shear might increase in the event that a developing cyclone moves close to a strong AEJ core, Braun suggests that the typical spatial relationship between the AEJ and tropical lows renders this possibility unlikely. Nevertheless, RM10 shows that the effect of shear on the entrainment of external air is a topic in need of further investigation.

These results show that the relationship among the SAL, AEJ, and developing tropical cyclones is not as straightforward as has been hypothesized by DV04, Wu (2007), Shu and Wu (2009), and others. For example, Fig. 7 of DV04 implies a negative relationship between the SAL and the intensity of seven different tropical cyclones that occurred during the 2000–01 seasons. While our results are consistent with negative SAL impacts during the weak stages of Erin and Felix in 2001, they are strongly incongruent with the assertion that the SAL caused Hurricanes Debby and Joyce in 2000 to dissipate. Furthermore, our results imply that the SAL likely inhibited intensification for a considerably shorter period of time than that indicated for Cindy (1999), Floyd (1999), and Chantal (2001). The results also strongly disagree with the claim in Shu and Wu (2009) that the SAL was directly responsible for the demise of Debby (2006). Ultimately, the nuanced relationship between storm intensity and the SAL shows that much care needs to be taken before drawing conclusions about the effect of the SAL on any particular cyclone. We therefore advocate more rigorous future analysis through both idealized and ensemble studies to more fully quantify the effect of the SAL on tropical cyclones in general.

Acknowledgments. The authors are grateful to Zhiyong Meng for help on the ensemble simulation and to helpful comments from three anonymous reviewers. Work by the first author began under the NASA Postdoctoral Program, sponsored by Oak Ridge Associated Universities through a contract with NASA and continued while the first author was employed at the Goddard Earth Sciences and Technology Center. This work was also supported by Dr. Ramesh Kakar at NASA Headquarters with funds from the NASA Hurricane Science Research Program. The simulations were conducted on NASA Center for Climate Simulation facilities.

REFERENCES

Barker, D. M., W. Huang, Y.-R. Guo, A. J. Bourgeois, and Q. N. Xiao, 2004: A three-dimensional variational data assimilation system for MM5: Implementation and initial results. *Mon. Wea. Rev.,* **132,** 897–914.

Bender, M. A., and I. Ginis, 2000: Real-case simulations of hurricane–ocean interaction using a high-resolution coupled model: Effects on hurricane intensity. *Mon. Wea. Rev.,* **128,** 917–946.

——, ——, and Y. Kurihara, 1993: Numerical simulations of tropical cylone–ocean interaction with a high-resolution coupled model. *J. Geophys. Res.,* **98,** 23 245–23 263.

Black, P. G., 1983: Ocean temperature changes induced by tropical cyclones. Ph.D. dissertation, The Pennsylvania State University, 278 pp.

Braun, S. A., 2010a: Reevaluating the role of the Saharan air layer in Atlantic tropical cyclogenesis and evolution. *Mon. Wea. Rev.,* **138,** 2007–2037.

——, 2010b: Comments on ''Atlantic tropical cyclogenesis processes during SOP-3 NAMMA in the GEOS-5 global data assimilation and forecast system.'' *J. Atmos. Sci.,* **67,** 2402–2410.

——, J. A. Sippel, and D. Nolan, 2011: The impact of dry midlevel air on hurricane intensity in idealized simulations with no mean flow. *J. Atmos. Sci.,* in press.

Carlson, T. N., and J. M. Prospero, 1972: The large-scale movement of Saharan air outbreaks over the northern equatorial Atlantic. *J. Appl. Meteor.,* **11,** 283–297.

Davis, C., and L. F. Bosart, 2002: Numerical simulations of the genesis of Hurricane Diana (1984). Part II: Sensitivity of track and intensity prediction. *Mon. Wea. Rev.,* **130,** 1100–1124.

——, and Coauthors, 2008: Prediction of landfalling hurricanes with the Advanced Hurricane WRF model. *Mon. Wea. Rev.,* **136,** 1990–2005.

DeMaria, M., J. A. Knaff, and B. H. Connell, 2001: A tropical cyclone genesis parameter for the tropical Atlantic. *Wea. Forecasting,* **16,** 219–233.

Doswell, C. A., III, and E. N. Rasmussen, 1994: The effect of neglecting the virtual temperature correction on CAPE calculations. *Wea. Forecasting,* **9,** 625–629.

Dudhia, J., 1989: Numerical study of convection observed during the winter monsoon experiment using a mesoscale two-dimensional model. *J. Atmos. Sci.,* **46,** 3077–3107.

Dunion, J. P., and C. S. Velden, 2004: The impact of the Saharan air layer on Atlantic tropical cyclone activity. *Bull. Amer. Meteor. Soc.,* **85,** 353–365.

Gray, W. M., 1968: Global view of the origin of tropical disturbances and storms. *Mon. Wea. Rev.,* **96,** 669–700.

Hakim, G. J., and R. D. Torn, 2008: Ensemble synoptic analysis. *Synoptic–Dynamic Meteorology and Weather Analysis and Forecasting: A Tribute to Fred Sanders, Meteor. Monogr.,* No. 55, Amer. Meteor. Soc., 147–162.

Hawblitzel, D. P., F. Zhang, Z. Meng, and C. A. Davis, 2007: Probabilistic evaluation of the dynamics and predictability of the mesoscale convective vortex of 10–13 June 2003. *Mon. Wea. Rev.,* **135,** 1544–1563.

Haynes, P. H., and M. E. McIntyre, 1987: On the evolution of vorticity and potential vorticity in the presence of diabatic heating and frictional or other forces. *J. Atmos. Sci.,* **44,** 828–841.

Hong, S.-Y., J. Dudhia, and S.-H. Chen, 2004: A revised approach to ice-microphysical processes for the bulk parameterization of cloud and precipitation. *Mon. Wea. Rev.,* **132,** 103–120.

Huffman, G. J., R. F. Adler, D. T. Bolvin, G. Gu, E. J. Nelkin, K. P. Bowman, E. F. Stocker, and D. B. Wolff, 2007: The TRMM multisatellite precipitation analysis: Quasi-global, multiyear, combined-sensor precipitation estimates at fine scale. *J. Hydrometeor.,* **8,** 38–55.

Jenkins, G. S., and A. Pratt, 2008: Saharan dust, lightning and tropical cyclones in the eastern tropical Atlantic during NAMMA-06. *Geophys. Res. Lett.,* **35,** L12804, doi:10.1029/2008GL033979.

——, ——, and A. Heymsfield, 2008: Possible linkages between Saharan dust and tropical cyclone rain band invigoration in the eastern Atlantic during NAMMA-06. *Geophys. Res. Lett.,* **35,** L08815, doi:10.1029/2008GL034072.

Jones, T. A., D. J. Cecil, and J. Dunion, 2007: The environmental and inner-core conditions governing the intensity of Hurricane Erin (2007). *Wea. Forecasting,* **22,** 708–725.

Kain, J. S., and J. M. Fritsch, 1990: A one-dimensional entraining/detraining plume model and its application in convective parameterization. *J. Atmos. Sci.,* **23,** 2784–2802.

——, and ——, 1993: Convective parameterization for mesoscale models: The Kain–Fritsch scheme. *The Representation of Cumulus Convection in Numerical Models. Meteor. Monogr.,* No. 46, Amer. Meteor. Soc., 165–170.

Karyampudi, V. M., and T. N. Carlson, 1988: Analysis and numerical simulations of the Saharan air layer and its effect on easterly wave disturbances. *J. Atmos. Sci.,* **45,** 3102–3136.

——, and H. F. Pierce, 2002: Synoptic-scale influence of the Saharan air layer on tropical cyclogenesis over the eastern Atlantic. *Mon. Wea. Rev.,* **130,** 3100–3128.

Lau, K. M., and J. M. Kim, 2007a: How nature foiled the 2006 hurricane forecasts. *Eos, Trans. Amer. Geophys. Union,* **88,** 105–107.

——, and ——, 2007b: Cooling of the Atlantic by Saharan dust. *Geophys. Res. Lett.,* **34,** L23811, doi:10.1029/2007GL031538.

Mlawer, E. J., S. J. Taubman, P. D. Brown, M. J. Iacono, and S. A. Clough, 1997: Radiative transfer for inhomogeneous atmosphere: RRTM, a validated correlated-*k* model for the longwave. *J. Geophys. Res.,* **102,** 16 663–16 682.

Noh, Y., W.-G. Cheon, S.-Y. Hong, and S. Raasch, 2003: Improvement of the *K*-profile model for the planetary boundary layer based on large eddy simulation data. *Bound.-Layer Meteor.,* **107,** 401–427.

Pratt, A. S., and J. L. Evans, 2009: Potential impacts of the Saharan air layer on numerical model forecasts of North Atlantic tropical cyclogenesis. *Wea. Forecasting,* **24,** 420–435.

Prospero, J. M., and T. N. Carlson, 1981: Saharan air outbreaks over the tropical North Atlantic. *Pure Appl. Geophys.,* **119,** 677–691.

Raymond, D. J., and H. Jiang, 1990: A theory for long-lived mesoscale convective systems. *J. Atmos. Sci.,* **47,** 3067–3077.

Reale, O., and W. K. Lau, 2010: Reply. *J. Atmos. Sci.,* **67,** 2411–2415.

——, ——, K.-M. Kim, and E. Brin, 2009: Atlantic tropical cyclogenetic processes during SOP-3 NAMMA in the GEOS-5 global data assimilation and forecast system. *J. Atmos. Sci.,* **66,** 3563–3578.

Reimer, M., and M. T. Montgomery, 2010: Simple kinematic models for the environmental interaction of tropical cyclones in vertical wind shear. *Atmos. Chem. Phys. Discuss.,* **10,** 28 057–28 107.

Shu, S., and L. Wu, 2009: Analysis of the influence of the Saharan air layer on tropical cyclone intensity using AIRS/Aqua data. *Geophys. Res. Lett.,* **36,** L09809, doi:10.1029/2009GL037634.

Sippel, J. A., and F. Zhang, 2008: A probabilistic analysis of the dynamics and predictability of tropical cyclogenesis. *J. Atmos. Sci.,* **65,** 3440–3459.

——, and ——, 2010: Factors affecting the predictability of Hurricane Humberto (2007). *J. Atmos. Sci.,* **67,** 1759–1778.

Skamarock, W. C., J. B. Klemp, J. Dudhia, D. O. Gill, D. M. Barker, W. Wang, and J. G. Powers, 2005: A description of the Advanced Research WRF version 2. NCAR Tech. Note NCAR/TN-468+STR, 88 pp.

Sun, D., K. M. Lau, and M. Kafatos, 2008: Contrasting the 2007 and 2005 hurricane seasons: Evidence of possible impacts of Saharan dry air and dust on tropical cyclone activity in the Atlantic basin. *Geophys. Res. Lett.,* **35,** L15405, doi:10.1029/2008GL034529.

Thorncroft, C. D., and B. J. Hoskins, 1994: An idealized study of African easterly waves. Part I: A linear view. *Quart. J. Roy. Meteor. Soc.,* **120,** 953–982.

Torn, R. D., 2010: Ensemble-based sensitivity analysis applied to African easterly waves. *Wea. Forecasting,* **25,** 61–78.

Vizy, E. K., and K. H. Cook, 2009: Tropical storm development from African easterly waves in the eastern Atlantic: A comparison of two successive waves using a regional model as part of NASA AMMA 2006. *J. Atmos. Sci.,* **66,** 3313–3334.

Wu, L., 2007: Impact of Saharan air layer on hurricane peak intensity. *Geophys. Res. Lett.,* **34,** L09802, doi:10.1029/2007GL029564.

——, S. A. Braun, J. J. Qu, and X. Hao, 2006: Simulating the formation of Hurricane Isabel (2003) with AIRS data. *Geophys. Res. Lett.,* **33,** L04804, doi:10.1029/2005GL024665.

Zhang, F., 2005: Dynamics and structure of mesoscale error covariance of a winter cyclone estimated through short-range ensemble forecasts. *Mon. Wea. Rev.,* **133,** 2876–2893.

——, and J. A. Sippel, 2009: Effects of moist convection on Hurricane predictability. *J. Atmos. Sci.,* **66,** 1944–1961.

Zipser, E. J., and Coauthors, 2009: The Saharan air layer and the fate of African easterly waves—NASA's AMMA field study of tropical cyclogenesis. *Bull. Amer. Meteor. Soc.,* **90,** 1137–1156.